9950-681

DRD No. SE-5
DRL No. 139

LARGE-AREA SHEET TASK
ADVANCED DENDRITIC WEB GROWTH DEVELOPMENT

C. S. Duncan, R. G. Seidensticker, J. P. McHugh,
R. H. Hopkins, D. Meier, and J. Schruben

Annual Report

October 23, 1980 to October 22, 1981

DOE/JPL-955843/82/1
DIST. CATEGORY UC-63

March 2, 1982

Contract No. 955843

The JPL Flat Plate Solar Array Project is sponsored by the U.S. Dept. of Energy and forms part of the Solar Photovoltaic Conversion Program to initiate a major effort toward the development of low-cost solar arrays. This work was performed for the Jet Propulsion Laboratory, California Institute of Technology, by agreement between NASA and DOE.

Westinghouse R&D Center
1310 Beulah Road
Pittsburgh, Pennsylvania 15235

DRD No. SE-5
DRL No. 139

LARGE-AREA SHEET TASK
ADVANCED DENDRITIC WEB GROWTH DEVELOPMENT

C. S. Duncan, R. G. Seidensticker, J. P. McHugh,
R. H. Hopkins, D. Meier, and J. Schruben

Annual Report

October 23, 1980 to October 22, 1981

DOE/JPL-955843/82/1
DIST. CATEGORY UC-63

March 2, 1982

Contract No. 955843

The JPL Flat Plate Solar Array Project is sponsored by the U.S. Dept. of Energy and forms part of the Solar Photovoltaic Conversion Program to initiate a major effort toward the development of low-cost solar arrays. This work was performed for the Jet Propulsion Laboratory, California Institute of Technology, by agreement between NASA and DOE.

Westinghouse R&D Center
1310 Beulah Road
Pittsburgh, Pennsylvania 15235

TABLE OF CONTENTS

LIST OF FIGURES..... v

1. SUMMARY..... 1

2. INTRODUCTION..... 2

3. PROGRESS IN WEB GROWTH RESEARCH..... 4

3.1 Development and Application of Thermal Stress Modeling..... 4

3.1.1 Basic Theory..... 4

3.1.2 Solution Methods..... 8

3.1.3 Stress and Buckling Calculations..... 10

3.1.3.1 WECAN Computer Code..... 10

3.1.3.2 Buckling Analysis..... 13

3.1.3.3 Stress and Buckling in J181 Ribbon..... 14

3.1.3.4 Investigation of Buckling Parameters..... 20

3.1.4 Generalized Design Guides..... 25

3.1.4.1 Residual Stress Index..... 27

3.1.4.2 Stress and Buckling..... 28

3.1.4.3 Application to the J352/J98M3C Growth Configurations..... 33

3.1.5 Zero Stress Profiles..... 38

3.1.6 Temperature Data for Modeling Calculations..... 40

3.1.6.1 Experimental Procedure..... 42

3.1.6.2 Results and Analysis..... 44

3.2 Experimental Web Growth..... 46

3.2.1 Advanced Growth Studies..... 46

3.2.1.1 Growth Velocity..... 48

3.2.1.2 Width Control..... 52

3.2.1.3 Melt Replenishment..... 53

3.2.1.4 Programmed Start of Growth..... 56

3.2.1.5 Long-Term Growth Stability..... 58
3.2.1.6 Test of Feed Stock Pellets from Kayex Corporation..... 62
3.3 Experimental Silicon Web Sheet Growth Machine..... 63
3.3.1 Purpose..... 63
3.3.2 General Description of Machine..... 63
3.3.3 Required Features for Sustained Steady State Web Growth..... 66
3.3.3.1 Constant Melt Level..... 68
3.3.3.2 Constant Temperature..... 71
3.3.3.3 Constant Width of Growth..... 71
3.3.3.4 Constant Web Thickness and Speed of Growth... 75
3.3.3.5 Programmed Start of Web Growth..... 75
3.3.4 Constant Melt Level..... 77
4. SILICON WEB ECONOMIC ANALYSIS UPDATE..... 78
5. SUMMARY AND CONCLUSIONS..... 79
5.1 Summary..... 79
5.2 Future Work..... 80
6. NEW TECHNOLOGY..... 81
7. REFERENCES 82
8. ACKNOWLEDGEMENTS..... 83

LIST OF FIGURES

Figure 1 Grid Used to Model Silicon Web for Stress Analysis..... 11

Figure 2 Perspective of Grid Used for Stress Calculation of..... 12
Silicon Web. Thickened Portion at Edge Represents
Dendrite.

Figure 3 The J-181 Baseline Lid and Top Shield Configuration..... 15

Figure 4 J181 Thermal Model..... 16

Figure 5 J181 Thermal Profile..... 17

Figure 6 Stress Distribution in 27 mm "J181" web..... 18

Figure 7 Calculated Shape of Buckled Web (half strip)..... 19

Figure 8 Stress Distributions for 33 mm "J181" Web 21

Figure 9 Stress Distributions for 39.5 mm "J181" Web 22

Figure 10 Buckled Shape for 39.5 mm "J181" Web (second..... 24
eigenvalue)

Figure 11 Buckling as Function of Width and Thickness for..... 26
J181 Lid Configuration

Figure 12 Schematic of Integration for Residual Stress Index..... 29
(RSI)

Figure 13 Stress Patterns in .010 cm Thick Ribbon..... 31

Figure 14 Schematic J352/J98M3C Configuration and Equivalent..... 34
Thermal Model Parameters

Figure 15 Synthetic Temperature Profiles..... 39

Figure 16 Comparison of Stress for "Ideal" and "Near Ideal"..... 41
Temperature Profiles

Figure 17 Configurations for System Temperature Measurement..... 43

LIST OF FIGURES (Cont.)

Figure 18 Typical Cross Sections of Recessed Lids for Growth..... 51
Speed Enhancement

Figure 19 Variation in Web Width with Length of Crystal Growth..... 54
for Lid Geometry Designed for Width Control

Figure 20 Typical Program Sequence for Web Growth Initiation..... 57

Figure 21 Temperature Control Transfer Circuit..... 59

Figure 22 Pull Speed Transfer Circuit..... 60

Figure 23 Experimental Web Growth Furnace -- Side View..... 64

Figure 24 Experimental Web Growth Furnace -- Front View..... 65

Figure 25 New Experimental Web Growth Furnace..... 67

Figure 26 Simplified Sketch of Melt Replenishment System..... 69

Figure 27 Polysilicon Pellets from Kayex Shot Tower..... 70
Left Side 0.4 to 2 mm. Right side 2.0 - 2.8 mm.

Figure 28 Block Diagram of Closed Loop Circuit for Control of..... 72
Melt Level

Figure 29 Block Diagram of Melt Replenishment Control System..... 73

Figure 30 Block Diagram of Silicon Web Temperature Control System.... 74

Figure 31 Web Growth Thickness at Constant Growth Speed With..... 76
and Without Melt Level Control

1. SUMMARY

During this reporting period, significant progress has been made in our understanding of the web growth process. Thermal models have been developed that accurately predict the thermally generated stresses in the web crystal which, if too high, cause the crystal to degenerate. The application of the modeling results to the design of low-stress experimental growth configurations will allow the growth of wider web crystals at higher growth velocities.

A new experimental web growth machine was constructed. This facility includes all the features necessary for carrying out growth experiments under steady state thermal conditions. Programmed growth initiation has been developed to give reproducible crystal starts. Width control permits the growth of long ribbons at constant width. Melt level is controlled to 0.1 mm or better. Thus, the capability exists to grow long web crystals of constant width and thickness with little operator intervention, and web growth experiments can now be performed with growth variables controlled to a degree not previously possible.

2. INTRODUCTION

Silicon dendritic web is a single crystal silicon ribbon material which provides substantial advantages for low-cost manufacture of solar cells. A significant feature of the process is the growth from a melt of silicon without constraining dies, resulting in an oriented single crystal ribbon having excellent surface features. In common with other more classical processes such as Czochralski growth, impurity rejection into the melt permits the use of less pure "solar grade" starting material without significantly affecting cell performance. A unique property of the dendritic web process is the growth of long ribbons of controllable width and thickness which not only facilitates automation of subsequent processing into solar cells, but also results in high material utilization since cutting and polishing are not required.

During the previous program (DOE/JPL Contract No. 954654), most of the component elements for the reproducible and steady state growth of high-quality web crystals were developed and demonstrated. Area throughputs greater than 25 cm^2/min were demonstrated for short periods of time. Melt replenishment for periods of up to 17 hours (a one-day growth cycle) was demonstrated. Thermal models were developed for calculating temperature distributions in the web crystal as a function of configuration parameters.

On the present contract and during this reporting period, three broad areas of work are emphasized:

1. The development of thermal stress models in order to understand the detailed parameters which generate buckling stresses. The model can then be used to guide the design of improved low-stress web growth configurations for experimental testing.

2. Experiments to increase our understanding of the effects of various parameters on the web growth process.
3. The construction of an experimental web growth machine which contains in a single unit all the mechanical and electronic features developed previously so that experiments can be carried out under tightly controlled conditions.

Thus, the principal objective of this work has been to expand our knowledge and understanding of both the theoretical and experimental aspects of the web growth process to provide a solid base for substantial improvements in both area throughput and web crystal quality.

3. PROGRESS IN WEB GROWTH RESEARCH

3.1 Development and Application of Thermal Stress Modeling

3.1.1 Basic Theory

Although surface tension forces may be the ultimate factor that limits the width of dendritic web crystals,[1] thermally generated stresses are presently a much more serious limitation. As the web crystal widens, the magnitude of the stress increases while at the same time the "stiffness" of the ribbon decreases until at some critical point the growing crystal buckles. Once the crystal has deformed, it is not only unsuitable for use in device fabrication, but also will lose its single crystal character. The overall goal of the thermal stress modeling work in this program is to reduce the thermal stresses in the growing web by changing the temperature profile in the ribbon through use of an appropriate thermal environment.

Thermal stresses have two major effects on the growth of ribbon crystals such as web: residual stresses which remain in the grown crystal and the deformation or "buckling" which occurs during growth.[2] In practice, the residual stresses can be controlled by tailoring the thermal environment near the growth front by proper design of the slot configuration in the lid and through control of the melt height.

Even when residual stresses are not a problem, buckling still occurs when the web has reached some critical combination of width and thickness. So far, control of the stresses causing buckling has not been obvious. Our goal in the present program is to identify the critical buckling stress magnitude, the temperature profile necessary to avoid deformation, and finally the growth configuration required to generate this profile.

Unlike the residual stress resulting from plastic deformation of the ribbon, the stresses causing buckling are affected by the temperature distribution away from the interface region. R. W. Gurtler[3] has modeled the stresses from two temperature distributions which were identical near the melt surface but different at greater distances. The first distribution decreased linearly along the length of the ribbon; there was no elastic stress and there would be no buckling. Unfortunately, this temperature distribution is unrealistic since absolute zero is reached a few centimeters from the growth front. The temperature decline could not be made more gradual without excessively slowing the growth rate.

The second temperature distribution was identical to the first near the growth front but parabolically approached ambient temperature instead of linearly reaching absolute zero; this temperature profile caused large elastic stresses.

Of course, the mere existence of thermal stresses in a growing web crystal does not automatically mean that the web will have residual stresses or deform during growth. In order for residual stress to be observed, the thermal stress must have exceeded the yield stress; for deformation to occur, the thermal stresses must exceed some critical buckling stress. A determination of the buckling stress criterion and the required temperature distribution would be a valuable guide in the design of high throughput growth configurations. The following sections review the mathematical formulation of both thermal stress generation and the ribbon deformation, and elucidate several approaches to solving the problems.

Stress model. The stresses in a thin ribbon of thickness t, length coordinate x, and width coordinate y, are related to the plane temperature distribution T (x,y) by means of the Airy stress function ϕ:

$$\sigma_{xx} = \frac{\partial^2 \phi}{\partial y^2}$$

$$\sigma_{xy} = - \partial^2 \phi / \partial_x \partial y \qquad (1)$$

$$\sigma_{yy} = \partial^2 \phi / \partial_x^2$$

where σ_{xx} is the longitudinal stress, σ_{xy} is the shear stress, and σ_{yy} the transverse stress. These stresses are determined from the temperature distribution via the differential equation

$$\Delta^2 \phi = -\alpha E \Delta T \qquad (2)$$

where α is the thermal expansion coefficient, E is the modulus of elasticity (Young's modulus),

$$\Delta \equiv \frac{\partial^2}{\partial x^2} + \frac{\partial^2}{\partial y^2} + \frac{\partial^2}{\partial z^2}$$

is the Laplacian or harmonic operator and Δ^2 is its square or the biharmonic operator. Boundary conditions require that both ϕ and its normal derivative should vanish on the growth front and on the edges of the web.

With proper shield design the web temperature should be nearly constant in the crosswise, or y, direction. For this case, $T = T(x)$, Boley and Wiener[4] have found an approximate series solution for equation 2 which is valid away from the melt surface. Numerical solutions can also be obtained by various techniques; for example, the Westinghouse WECAN finite element code has been used to solve for the stress distribution both near and far from the growth front with an arbitrary temperature distribution for input.[2]

Buckling Model. Whether or not the stresses determined by equation 2 would cause buckling depends on another differential equation which also involves the biharmonic operator[5]:

$$\frac{t^3 D \Delta^2 w}{12(1-\nu^2)} = \sigma_{xx} \frac{\partial^2 w}{\partial x^2} + \sigma_{yy} \frac{\partial^2 w}{\partial y^2} + 2\sigma_{xy} \frac{\partial^2 w}{\partial x \partial y} \qquad (3)$$

where ν is Poisson's ratio, E is Young's modulus, and w(x,y) is the transverse deflection (z direction) of a buckled thin plate of thickness t. The system of equations 6, 7, and 8 under the appropriate boundary conditions form the mathematical model of buckling in silicon web growth.

Since the web edges consist of dendrites which are less flexible than the web itself, the closest model for the boundary conditions would seem to be edges supported by elastic beams[5]:

$$EI \frac{\partial^4 w}{\partial x^4} = \pm D \left| \frac{\partial^3 w}{\partial y^3} + (2-\nu) \frac{\partial^3 w}{\partial x^2 \partial y} \right| + A \sigma_{xx} \frac{\partial^2 w}{\partial x^2} \qquad (4)$$

on the edges $y = \pm c$, where EI is the flexural rigidity of the dendrite, A is the cross-sectional area of the dendrite, and $D = ET^3/12(1-\nu^2)$ is the flexural rigidity of the plate or web. Here we have added the last term on the right side of equation 4 to account for the longitudinal variation of σ_{xx}. Equation 4 accounts for the twisting moments and the vertical shearing forces at the edges. The bending moments are considered in an additional boundary condition:

$$I C \frac{\partial}{\partial x} \left(\frac{\partial^2 w}{\partial x \partial y}\right) = D \left(\frac{\partial^2 w}{\partial x^2} + \nu \frac{\partial^2 w}{\partial y^2}\right) \qquad (5)$$

on $y = \pm C$, where C is the torsional rigidity of the dendrite.

For the edge of the initial button, boundary conditions similar to equations 4 and 5 would be appropriate when the growth has recently begun. After the web is long enough to wrap around the pickup reel, the leading edge of the web would be fixed and the boundary conditions would then be

$$w = \partial w / \partial x = 0 \qquad (6)$$

Finally, at the growth front x = 0, the edge is free and the boundary conditions are:

$$\partial^3 w/\partial x^3 + (2-\nu)\ \partial^3 w/\partial x \partial y^2 = 0$$
$$\partial^2 w/\partial x^2 + \nu \partial^2 w/\partial y^2 = 0 \qquad (7)$$

3.1.2 Solution Methods

The WECAN program can solve equations 1 to 7 for any arbitrary temperature distribution. (The problem of designing a furnace configuration to produce a desired temperature distribution will be considered after it is learned what the desired distribution is.) Unfortunately, finding a solution for equations 1 to 3 does not solve the buckling problem. In fact, the trivial solution, $w \equiv 0$, is such a solution; it represents the nonbuckled state. As long as no other solution exists, there can be no buckling. The problem thus is to determine the range of temperature distributions which induce sufficiently low stresses such that equations 3 to 7 have a unique solution, $w = 0$. This range of temperature profiles will give leeway for proper silicon growth. We shall discuss four possible ways to approach this problem:

1. The WECAN computer program has the capability to solve eigenvalue problems, and we can approximate the buckling problem as an eigenvalue problem by varying the stresses in a fixed proportion; i.e., let

$$\sigma_{xx} = \lambda \sigma^{o}_{xx}$$

$$\sigma_{yy} = \lambda \sigma^{o}_{yy}$$

$$\sigma_{xy} = \lambda \sigma^{o}_{xy}$$

where σ^{o}_{xx}, σ^{o}_{vy}, σ^{o}_{xy} are the stresses determined from equations 1 and 2 for some typical temperature distribution $T^{o}(x)$. WECAN can then

determine the values of λ for which equations 3 to 7 have a unique trivial solution. For these values of λ, any of the temperature distributions $\lambda T^{o}(x) + ax + b$ (a and b are independent of x and chosen to satisfy appropriate boundary conditions), would provide buckle-free silicon web growth. Notice that the second derivative of any of these distributions is proportional to that of the initial temperature distribution. Repetition of the above method for one or more initial temperature distributions (which are not proportional) could give some indication of the range of temperature distributions for which web growth would be stable.

2. Timoshenko and Gere[5] show how the eigenvalue problem mentioned in equation 1 can be solved as a minimization problem when series solutions to equations 3 to 7 can be determined. They give series expansions for similar boundary problems, and it is possible that these might be adapted to the problem at hand.

3. Similar to the energy method implied in equation 2 is functional analysis theory[6] for the uniqueness of solutions to the buckling differential equation. This theory may provide additional insight for determining the range of desirable temperature distributions for web growth.

4. Integral equations provide powerful methods for obtaining solutions to equation 3[7]; however, the complicated boundary conditions, equations 4 to 7, make the analysis too difficult to pursue for the present.

Conclusion: Although the analytic techniques investigated offer great power and generality for establishing buckling criteria, they would require considerable additional development before they could be applied to our specific problem. Thus, for the present, it would appear that finite element numerical analysis, while less general in scope, is nevertheless the most effective approach for investigating thermal stress and critical buckling conditions in dendritic web crystals.

3.1.3 Stress and Buckling Calculations

3.1.3.1 WECAN Computer Code

The Westinghouse finite element code, WECAN, has been used previously for the relatively simple problem of calculating thermal stresses in a two-dimensional representation of dendritic web. In the present work, we are employing the full capabilities of the code to calculate the critical buckling stresses in a web crystal modeled as a three-dimensional bar including the stiffening effect of the supporting dendrites. The required three-dimensional program uses nodal points at the intersection points of each of the finite element parallelepipeds and also at points midway between them. Further, for the buckling analysis each nodal point is allowed three degrees of freedom.

To reduce computer time and cost, the grid size can be minimized by dividing the ribbon into only the number of finite elements needed for reasonable computational accuracy. While this number cannot be determined a priori, at least the placement of the finite elements should be arranged so as to have the finest grid structure in the region of maximum temperature and stress variation. For the dendritic web problem, this region is near the melt surface. A nonuniform grid can make the variation of stress across each finite element more nearly zero than can be done with a uniform grid. Although WECAN cannot handle large variations in grid spacing from one element to the next, it can accommodate a grid with element size varying as a geometric progression. Such a grid for the silicon web is shown in Figure 1; the elements next to the surface are one-eighth as long as the elements at the other end. A perspective view of a section of the mesh is illustrated in Figure 2 to show the modeling of the bounding dendrites.

In addition to the finite element grid, WECAN requires a temperature input for each nodal point. The temperature distribution along the ribbon cannot be measured easily but is obtained by integrating the heat conduction equation for a specific furnace lid and shield geometry.[8] The uniform step size used in the previous

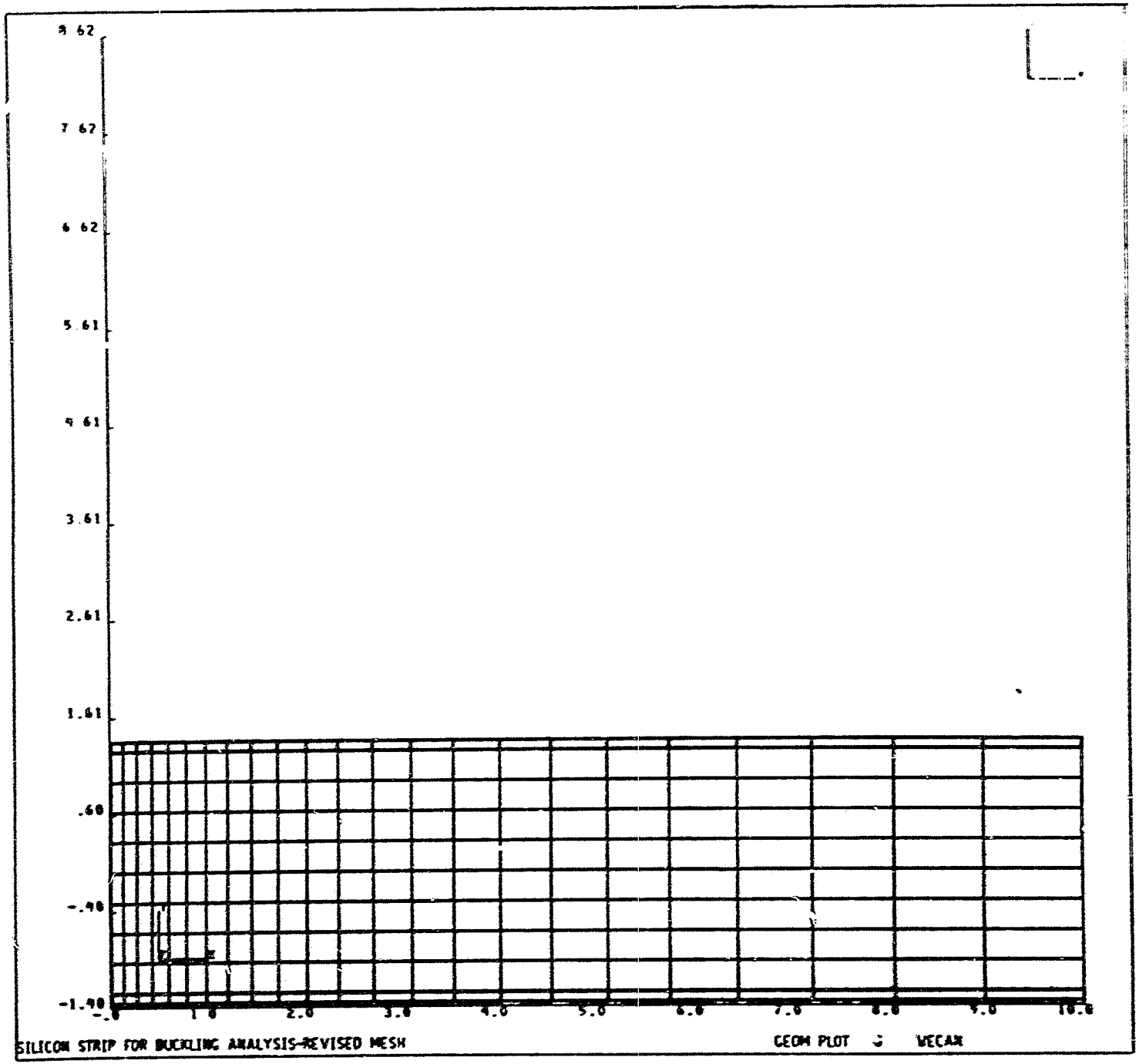

Figure 1 — Grid Used to Model Silicon Web for Stress Analysis

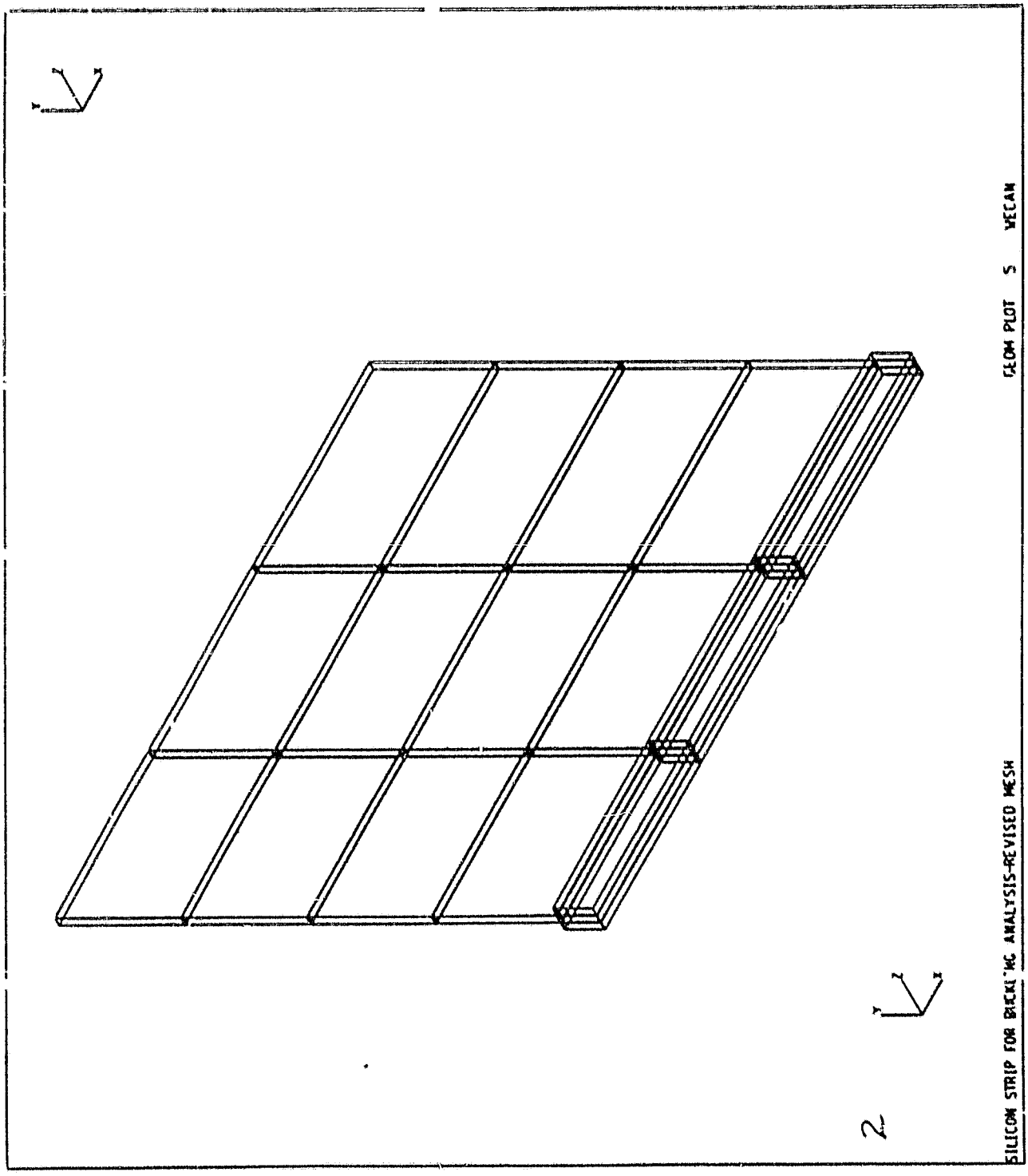

Figure 2 — Perspective of Grid Used for Stress Calculation of Silicon Web. Thickened Portion at Edge Represents Dendrite.

integration algorithm does not match with the geometrically varying grid used with WECAN, and modification to match the points led to numerical instabilities. A solution was finally obtained by interpolation of the results of the uniform step integration.

3.1.3.2 Buckling Analysis

Buckling occurs as a sudden deformation in the planar silicon strip when the thermal stresses reach some critical magnitude. Mathematically, buckling can be represented as an eigenvalue problem where the critical stress distribution is represented by an eigenvalue and the buckled shape by an eigenvector. For buckling problems, WECAN solves an equation of the form

$$[K]\ \{\Delta\} = \lambda\ [K_s]\ \{\Delta\} \qquad (8)$$

where $[K]$ is the conventional stiffness matrix, $[K_s]$ is the initial stress matrix resulting from a given temperature distribution, and $\{\Delta\}$ is a vector containing the unknown displacements of the ribbon surface. A solution parameter to the above equation, λ, is an eigenvalue and the corresponding $\{\Delta\}$ is an eigenvector; there can be many eigenvalues for a given equation. The smallest positive one is the most significant, since the product of it with $[K_s]$ is the weakest stress distribution for which buckling occurs. Negative eigenvalues imply a reversal of the sign of the stress distribution or a heating instead of a cooling of the ribbon from the melt surface. Although negative eigenvalues may be obtained mathematically for some $[K_s]$, they are not physically meaningful. We shall discuss these concepts further in terms of a specific example -- ribbon grown using the J181 lid and shield configuration.

3.1.3.3 Stress and Buckling in J181 Ribbon

J181 ribbon is grown out of a silicon melt covered and shielded as illustrated in Figure 3. The corresponding thermal model is shown in Figure 4; the temperatures are measured data.[9] A previously developed thermal modeling program[10] was used to calculate the temperature distribution in the growing web resulting from this growth geometry; the result is shown in Figure 5.* This temperature distribution was used as the input to WECAN to calculate the stresses in a 10 cm long and 150 μm thick ribbon. The width of the web between the dendrites was taken as 2.5 cm for a total ribbon width of 2.7 cm. The WECAN code then calculated the x stress along the length of the ribbon, the y stress across the width of the ribbon, and the xy shear stress. Figure 6 shows the stress contours for these three components. The top edge of the strip is the outer edge of the dendrite, the left edge is the melt surface, the right edge is 10 cm from the melt surface, and the bottom edge is the centerline of the ribbon with the stresses symmetric about this line. These stresses determine the matrix $[K_s]$ of equation 1, since other components of the stress tenor vanish for thin ribbons.

Using the initial stress matrix $[K_s]$, WECAN then solved equation 13 for the eigenvalue $\lambda = 1.65$, and its corresponding eigenvector or buckled shape is illustrated in Figure 7. Since λ is greater than unity, this ribbon would not have buckled -- all the stresses would have to be increased by a factor of 1.65 to obtain the illustrated deformation. The stability of 150 μm thick and 27 mm wide web agrees with growth experience with the J181 configuration.

In the actual growth apparatus, the ribbon is actually about 50 cm long, rather than 10 cm, before it is wound up on the reel. The

* Only temperature for distances less than 10 cm from the melt was calculated using the previous program. An asymptotic procedure, to be discussed later, was used for greater distances.

Dwg. 7702A61

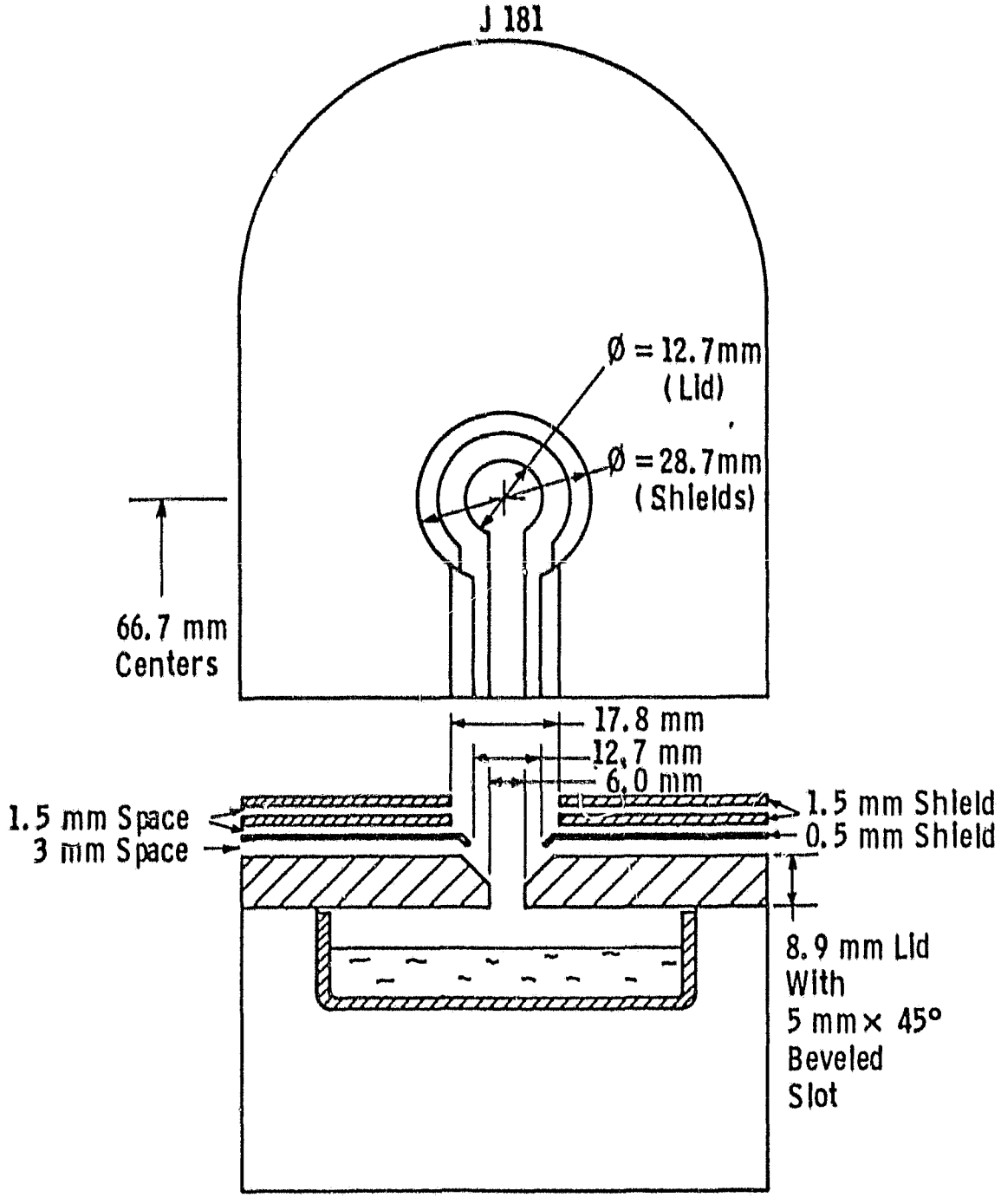

Figure 3 -- The J-181 Baseline Lid and Top Shield Configuration

Dwg.7709A12

TC	TS	TBEVEL	TAS	TLID	ZD	ZH
1623	1460	.6	1213	1.0	1.35	1.85

Dimensions in CM

Temp. in °K

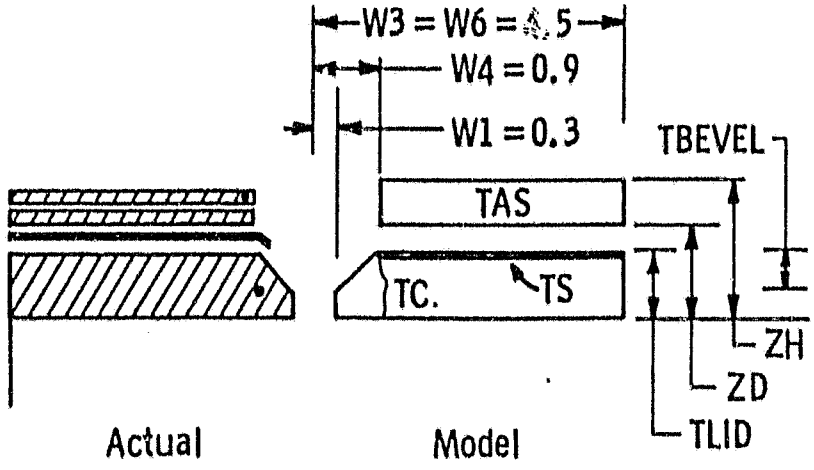

• Thermocouple Location

Figure 4 -- J181 Thermal Model

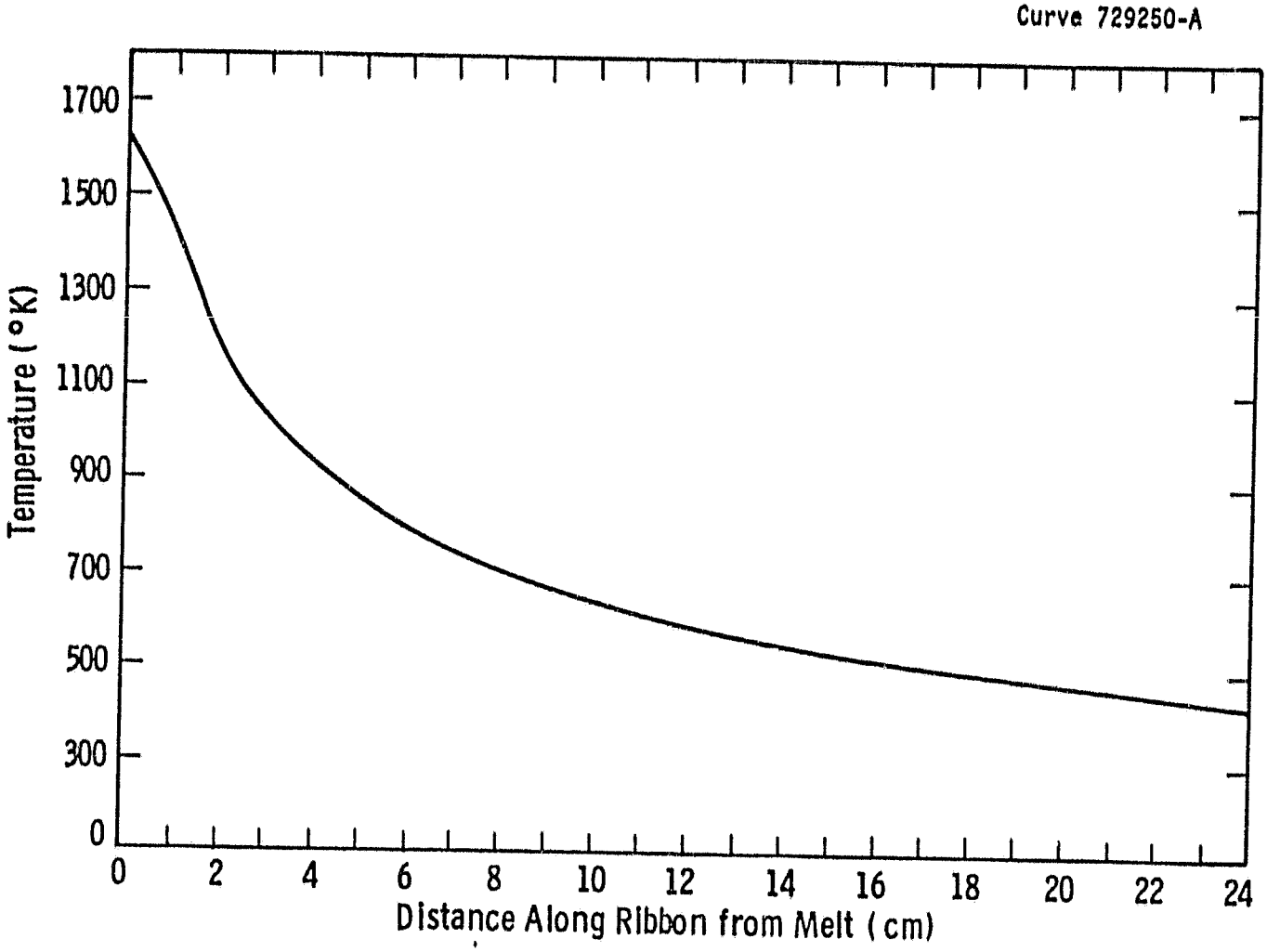

Figure 5 — J181 Thermal Profile

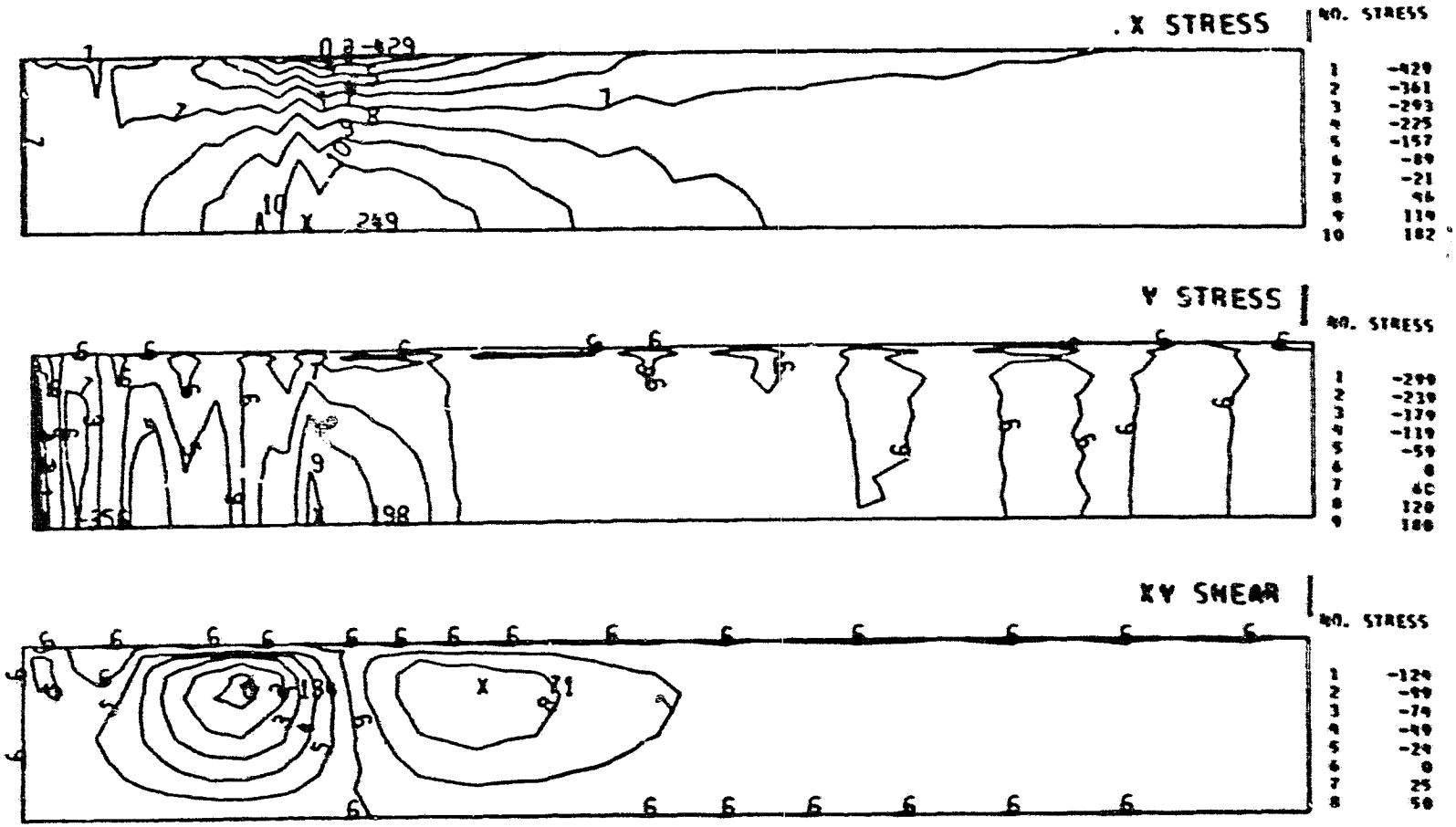

Figure 6 — Stress Distribution in 27 mm "J181" web

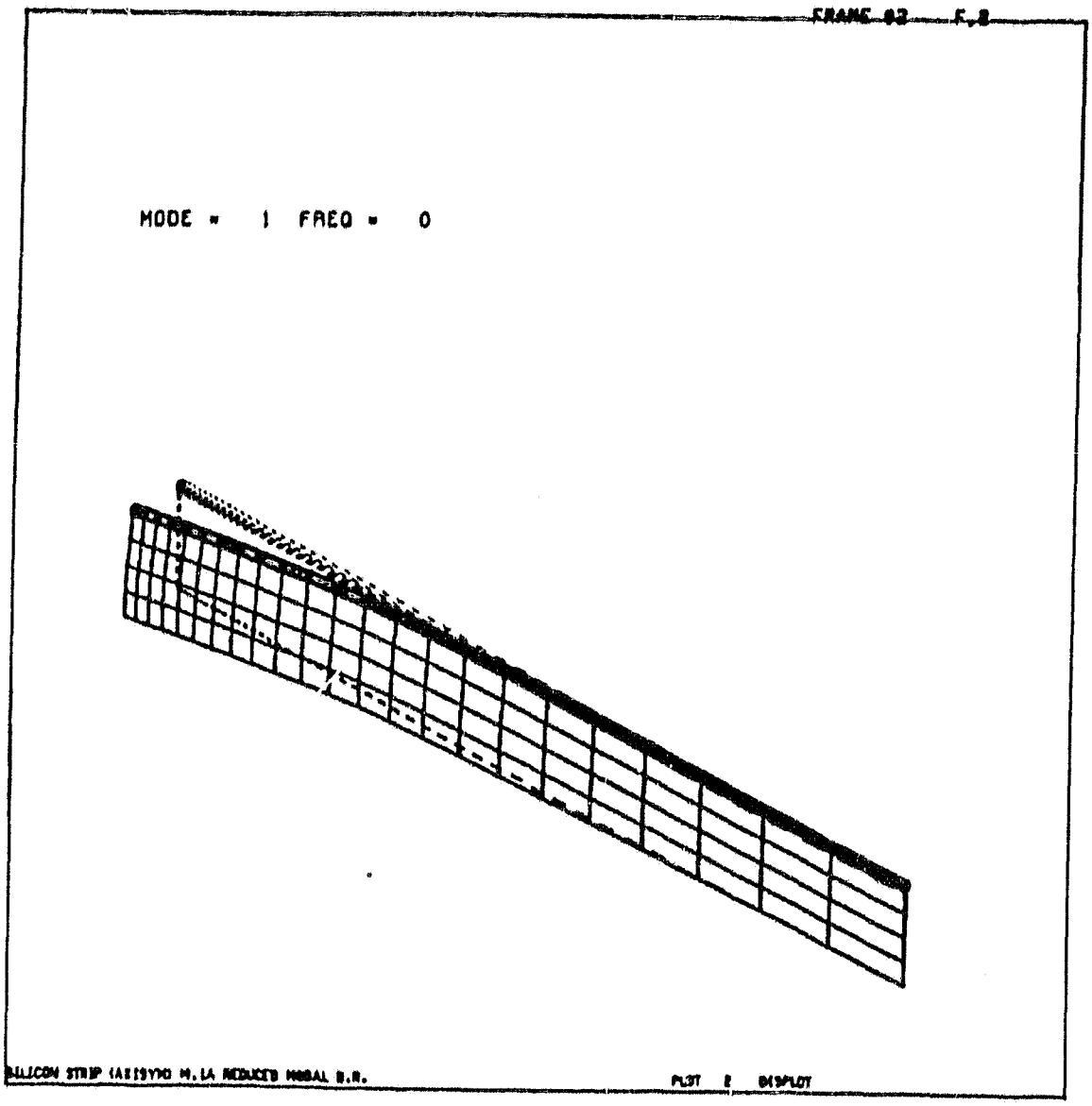

Figure 7 -- Calculated Shape of Buckled Web (half strip).

computer used for the WECAN analysis does not have sufficient storage capacity to model this length, unless it were divided up into very large elements. Since the largest stresses occur within only about 3 cm of the melt interface, it was felt that a 10 cm long model would be adequate for the present purposes. Nevertheless, we added three rows of elements for a total length of 13.6 cm to check the invariance of the eigenvalue λ. This longer ribbon was found to require slightly more stress for buckling with $\lambda = 1.67$. We felt that this 0.02 increase in λ was within experimental error and insufficient to warrant the additional computer time.

Not only is more computer time necessary to evaluate longer models, but the temperature input data is more difficult to obtain. The temperature integration becomes inaccurate at large distances away from the melt surface. An asymptotic method was used to find the temperature of the ribbon away from the melt, as graphed in Figure 5. This method will be discussed in an appendix to a future report.

3.1.3.4 Investigation of Buckling Parameters

With some assurance that the WECAN buckling model is reasonable, we proceeded to use it to investigate the effect of ribbon width and thickness on the buckling resistance. These parameters are of prime importance in the eventual goal of designing a growth geometry which will grow wide, thin (i.e., fast) web crystals.

Width Effects. We chose two widths, 33 mm and 39.5 mm, to compare with the 27 mm J181 ribbon which was initially modeled. The stress contours for these widths are shown in Figures 8 and 9. According to Boley and Wiener's approximation,[4] the shear stress should vanish on the centerline and it does in the numerical results. The x- and y-stresses, however, do not exhibit the expected width dependence: $\sigma_x \sim w^2$ and $\sigma_y \sim w^4$. Examining the point of maximum stress along the centerline, we find instead that $\sigma_x \sim w^{.91}$ and $\sigma_y \sim w^{1.28}$ with a slight variation in the exponent depending on which of the width cases are

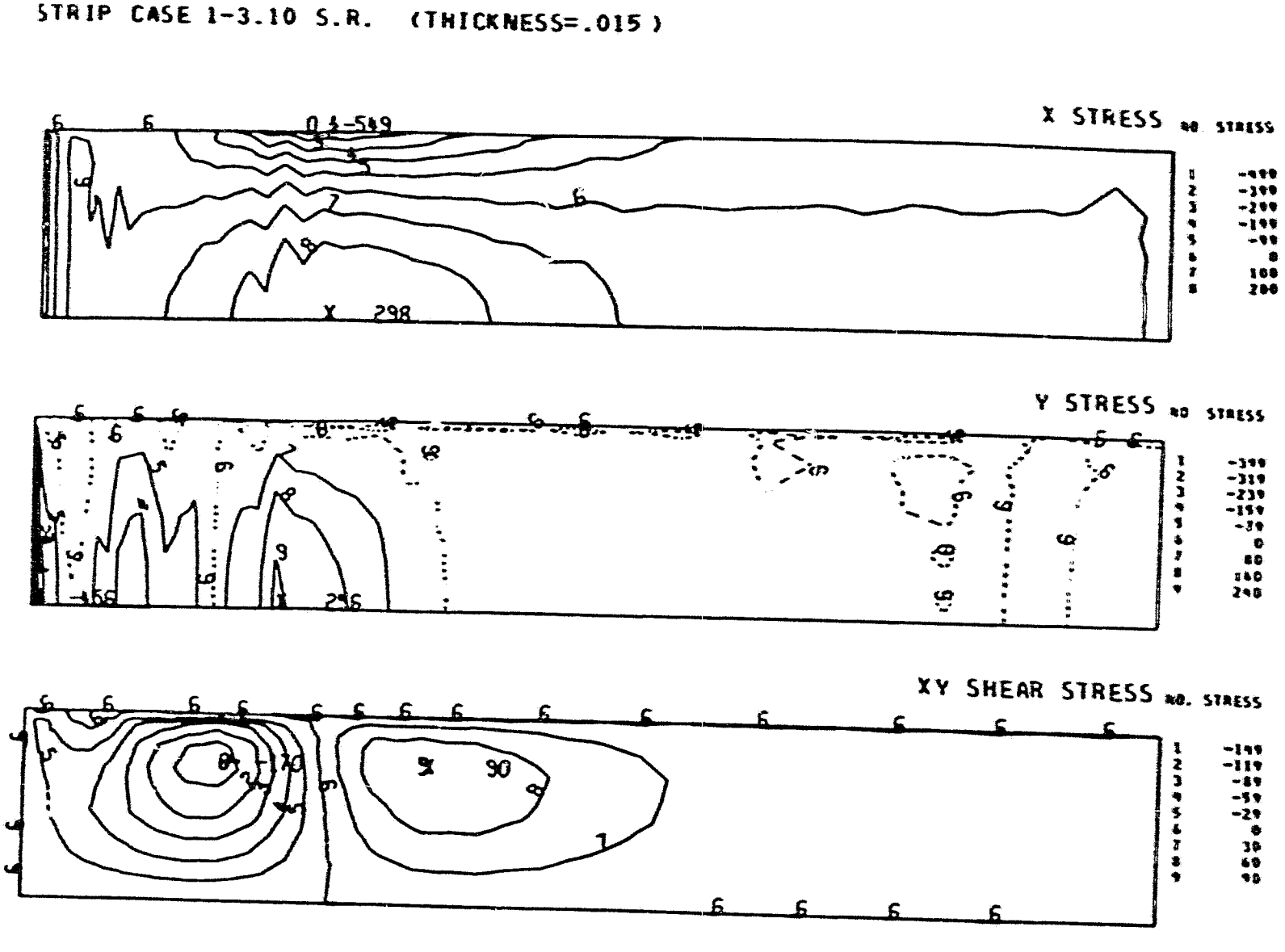

Figure 8 — Stress Distributions for 33 mm "J181" Web

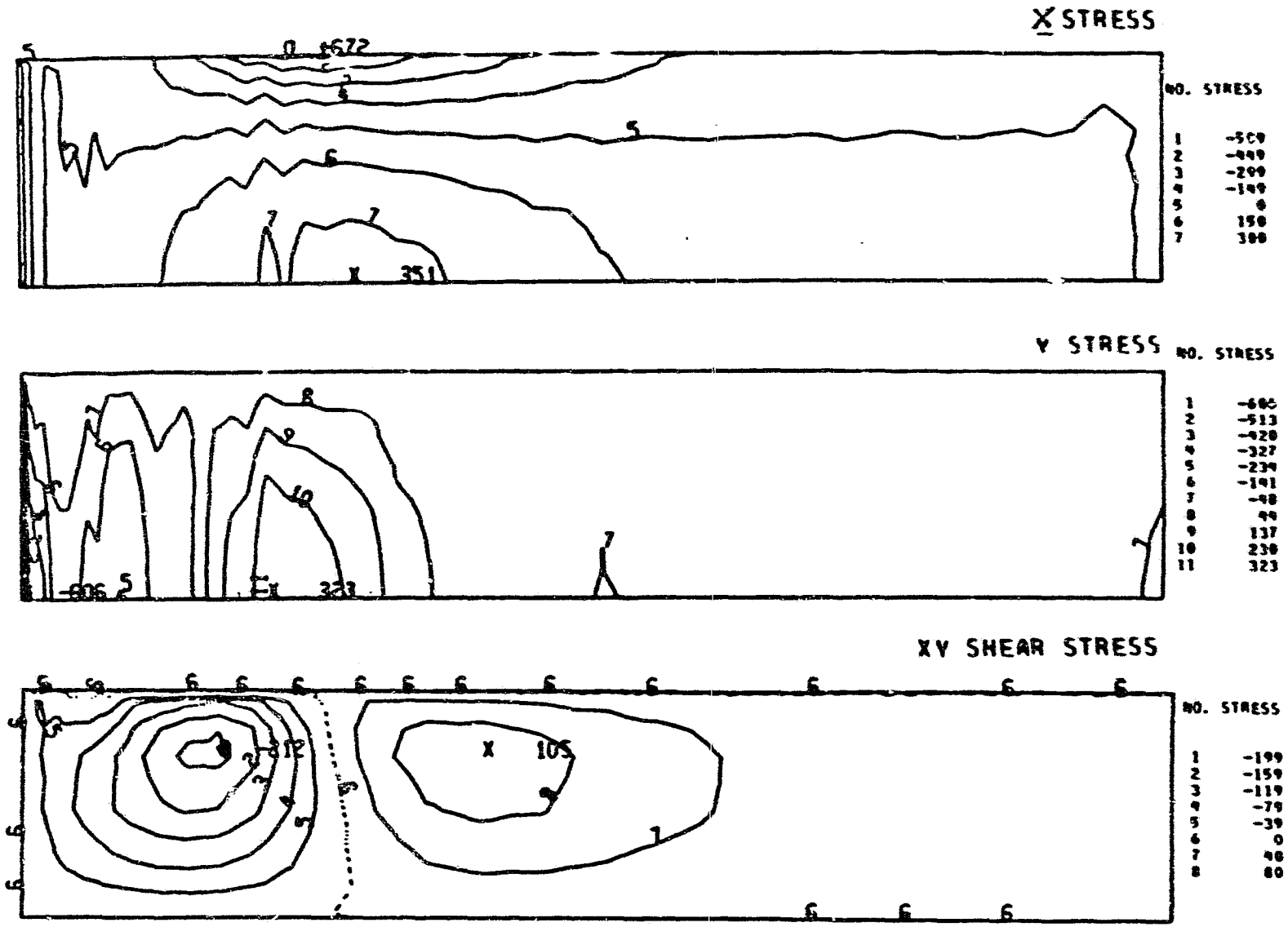

Figure 9 — Stress Distributions for 39.5 mm "J181" Web

compared. The fact that the exponent is not equal to 2 for the x-stress is not too surprising since Boley and Wiener's approximation[11] is best at distances far away from the ends of a ribbon, whereas in our case the maximum stress is only about a ribbon width away from the melt end. For this same reason, it cannot be expected that the x-stress at the dendrite edge should be double that at the centerline and opposite in sign as predicted by the approximate theory.[4] It is also true that the dendrites affect the stress pattern. The ratios of the minimum x-stress on the dendrite edge to the maximum x-stress on the centerline are -1.7, -1.8, and -1.9 for the 27 mm, 33 mm, and 39.5 mm widths of ribbon, respectively. The increasing magnitude of this ratio for increasing widths probably reflects the decreasing stiffness effect of the dendrite since the dendrite width is held constant at 1 mm.

The smallest positive eigenvalues for the 33 and 39.5 mm ribbons are $\lambda = 0.797$ and $\lambda = 0.418$, respectively. Their corresponding eigenvectors (shapes) are very similar to that shown in Figure 7. Since these eigenvalues are less than unity, the ribbon would buckle before its width could be increased from 27 mm to 33 mm. If we assume that λ varies inversely as the n_{th} power of the width, then $n = 3.63$ for a comparison of the 27 mm and 33 mm widths; using $n = 3.63$ to interpolate, we find that the ribbon should buckle ($\lambda = 1$) at $w = 31$ mm. This agrees well with growth experience for web crystals grown from a J181 configuration.

The 39.5 mm ribbon has another eigenvalue less than unity: $\lambda = 0.95$. Its buckled shape is pictured in Figure 10. This wide ribbon could buckle like this or in the shape of its first order mode ($\lambda = 0.418$). The first order mode is the more likely one to occur with the higher order mode occuring only if physical constraints should damp the lower mode.

Thickness Effects. We evaluated two additional ribbon sizes: 100 μm thick by 27 mm wide and 300 μm thick by 39.5 mm wide. From plots of the stress distributions, we find that the ratios of minimum to

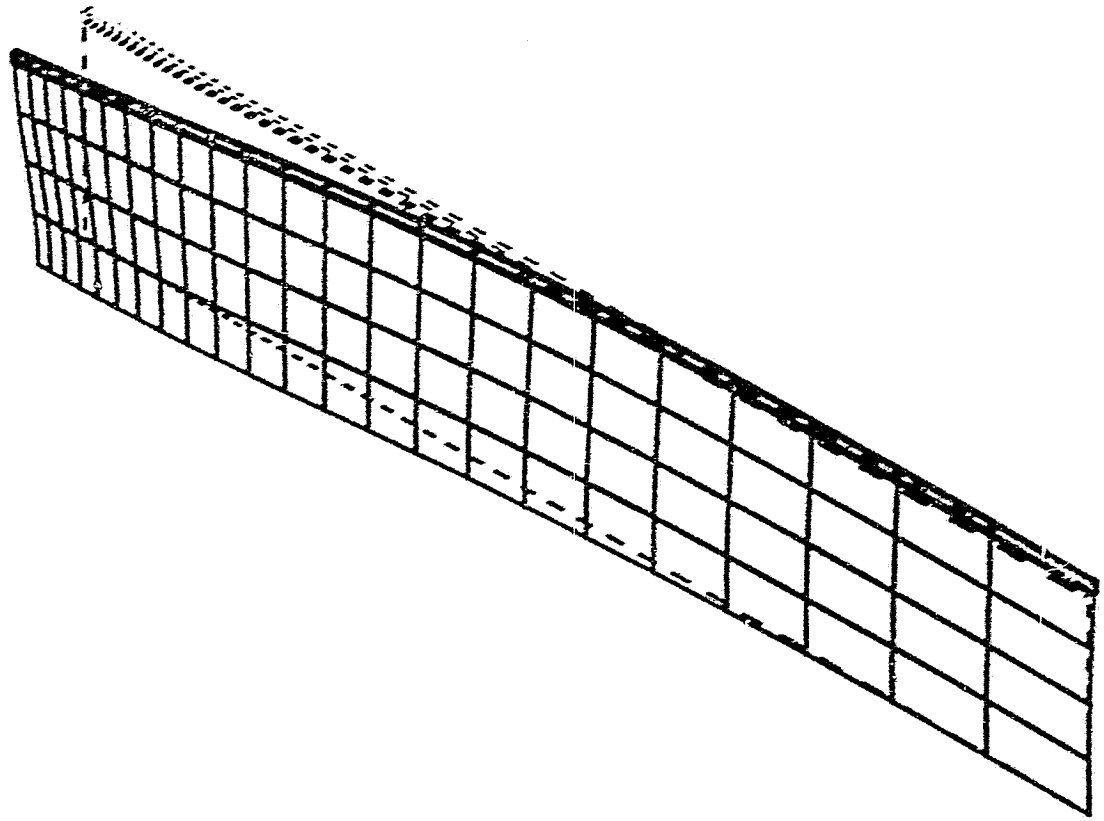

Figure 10 — Buckled Shape for 39.5 mm "J181" Web (second eigenvalue)

maximum x-stress are -1.4 for the smaller and -2.3 for the larger ribbon. In the 300 μm by 39.5 mm ribbon, the minimum x-stress does not occur at the same distance from the melt surface as that of the maximum x-stress. For this case, if we choose a point on the dendrite at the same distance from the melt as the point where the maximum x-stress occurs on the centerline, then the ratio of dendrite to centerline stress is -2.1, which is very close to the predicted value of -2. Again we find that the ratio of dendrite to centerline stress is closest to -2 in those ribbons in which the dendrites have the least volume relative to the rest of the ribbon. The difference between the thickness of the dendrite and that of the ribbon remains constant as the ribbon thickness is varied, so that the dendrite's relative volume is smallest for wide, thick ribbons.

The smallest eigenvalue for the 100 μm by 27 mm ribbon is 1.11, while that for the 300 μm by 39.5 mm ribbon is 1.06. Thus, the 27 mm wide ribbon would buckle when its thickness decreases to some value less than 100 μm, and the 39.5 mm ribbon would buckle at some critical value between 150 μm and 300 μm. To determine the critical thickness, we interpolate using the assumption that the eigenvalue λ is proportional to the mth power of the thickness; for our cases, $m = 0.98$ for the 27 mm ribbon and $m = 1.34$ for the 39.5 mm wide ribbon. Using these m's, we find that the 27 mm ribbon should buckle at 90 μm and the 39.5 mm ribbon should buckle at 287 μm. These points, together with the 150 μm thickness for a 31 mm width are plotted in Figure 11. The regions of stability (thick or narrow web) and instability (wide or thin web) are separated by an essentially straight line. Points determined by calculating the width at which a 100 μm or 300 μm thick web would buckle also lie on this line. The simplicity of this result is rather surprising in light of the complexity of the buckling mechanism.

3.1.4 Generalized Design Guides

The preceding sections have presented the development and application of finite element methods for calculating thermal stresses

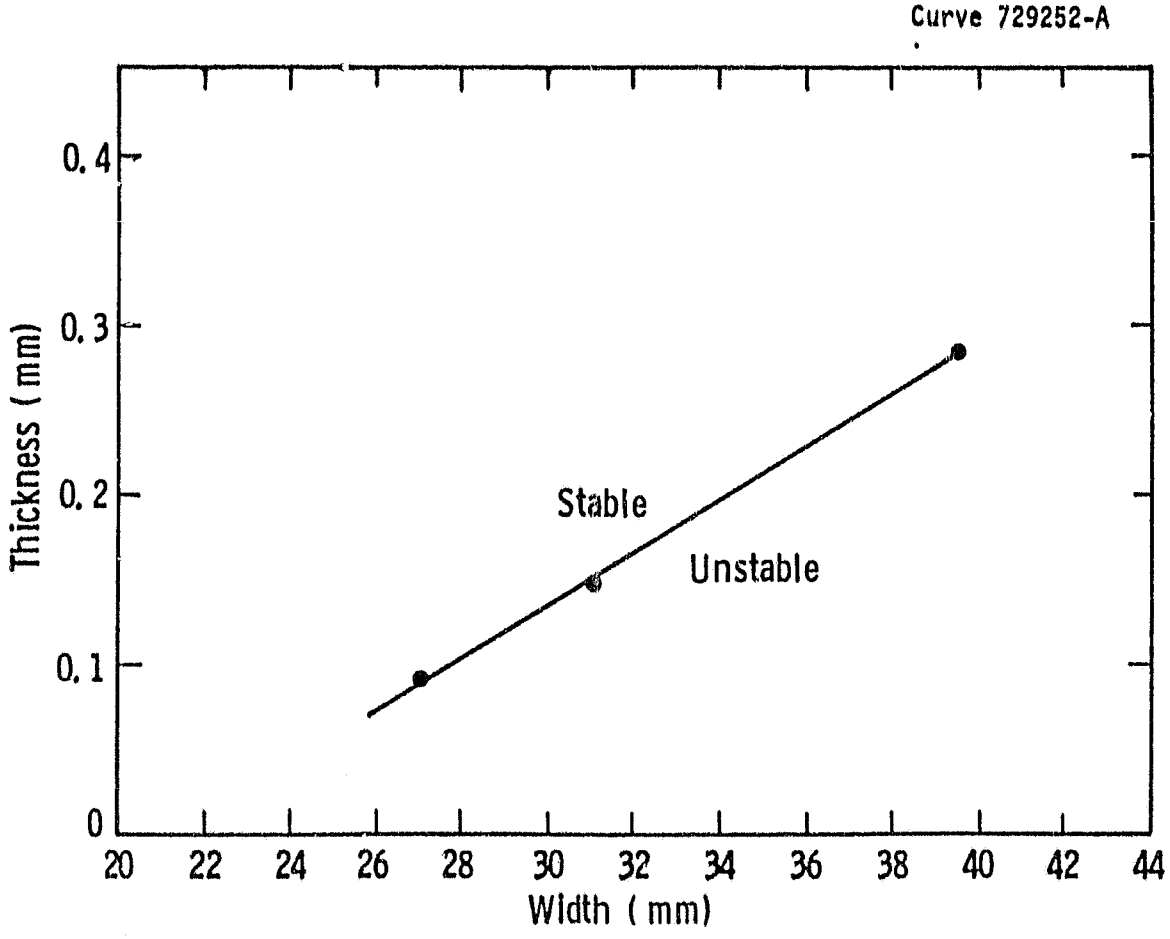

Figure 11 -- Buckling as Function of Width and Thickness for J181 Lid Configuration

and also critical buckling conditions during the growth of silicon dendritic web. Evaluation of the buckling behavior of a given growth configuration is a three-step process: (1) calculation of the temperature profile in the web crystal using the temperature thermal code; (2) calculation of thermal stresses for a three-dimensional model; and (3) calculation of the buckling eigenvalues. In practice, steps 2 and 3 are performed in the same computer program; however, this computation is rather lengthy and complex. By comparison, calculating the stresses in a two-dimensional model is relatively simple. It would be desirable to have some qualitative or semiquantitative guidelines to evaluate a growth configuration based only on two-dimensional stress calculations. This section presents some preliminary work on such guidelines both for residual stress and for critical buckling stresses. The results are illustrated by consideration of the J98M3/J352 configuration.

3.1.4.1 Residual Stress Index

Up to now, our analysis has emphasized thermal stress buckling due to its limiting effect on ribbon width. Residual stress, on the other hand, may not as directly affect the ribbon growth but it can certainly affect the ease of fabrication of the ribbon into devices. Consequently, we must also consider residual stress when evaluating various lid and shield configurations.

Although the generation of residual stress during crystal growth is a complicated visco-elastic process, hopefully a simple model will be sufficient to predict growth behavior, at least on a comparative basis. In simple terms, residual stress occurs when the thermal stress exceeds the yield stress for silicon. In the high-temperature region near the growth front, the transverse stress, σ_y, is the only stress component of any magnitude, and we shall use the following empirical relation for the yield stress[12]:

$$\sigma_{YS} = 2.57 \times 10^{-11} \exp (49459/T) \text{ dyn/cm}^2 \quad (9)$$

where T is the temperature in Kelvin.

The amount of residual stress should depend on the magnitude of the difference between the lateral stress and the yield stress and also on the length of time that the material is in that condition. Thus, to obtain some approximation to the residual stress, we define a Residual Stress Index (RSI) as the area between the yield and transverse stress curves plotted as functions of distance from the melt. For this purpose, the transverse stress at the centerline is used since it is largest in this region. Figure 12 illustrates the area concerned using case 10-6 (next section) as an example.

For computational purposes, the stress functions are approximated by line segments connecting data points: (x_i,y_i) and (x_i,z_i); $i = 0, \ldots, n$. The x_i's are distances from the melt, the y_i's are the ordinates of the yield stress, and the z_i's are the ordinates of the transverse stress; n is the smallest value of i such that $|y_i| > z_i|$. The Residual Stress Index may thus be computed as the sum of the areas of trapezoids and a triangle.

$$RSI = 1/2 \sum_{j=1}^{n-1} (x_j - x_{j-1}) (y_{j-1} - z_{j-1} + y_j - z_j) + 1/2 (y_{n-1} - z_{n-1})^2 (x_n - x_{n-1}) / (y_{n-1} - y_n + z_n - z_{n-1}) \quad (10)$$

In the case illustrated, the RSI = 41.5 Mdyn/cm; the magnitude of this number indicates the likelihood of undesirable residual stress.

3.1.4.2 Stress and Buckling

It would be convenient to have an index for buckling analogous to the Residual Stress Index. No single number, however, could be

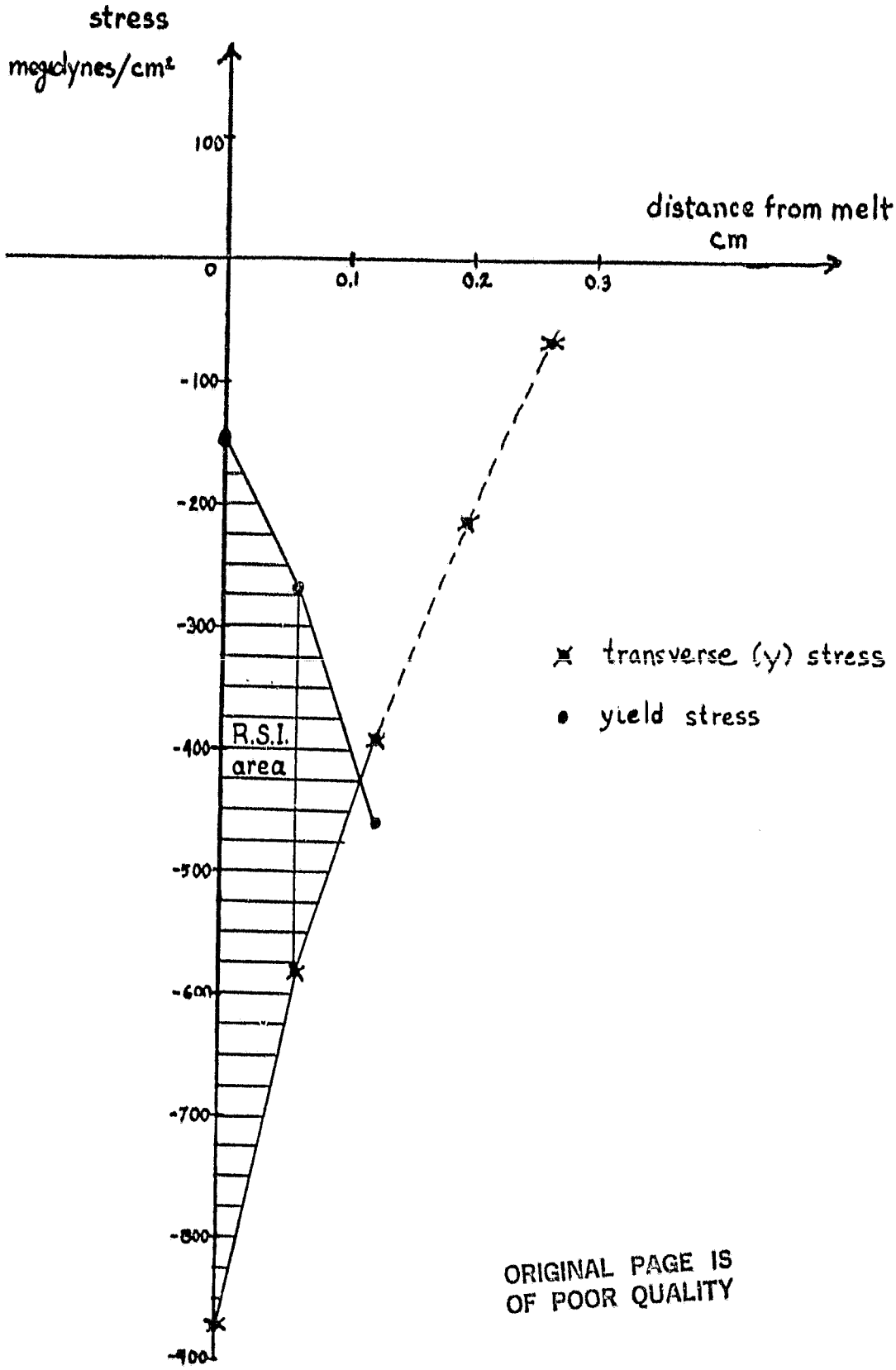

Figure 12 -- Schematic of Integration for Residual Stress Index (RSI)

expected to predict buckling in general. The stress patterns determine the buckling for a given ribbon size. With the goal of understanding which features of the stress patterns are most important, we examined the variational formula for the buckling eigenvalue, λ.[5]

$$\lambda = \frac{D \int\int [(w_{xx} + w_{yy})^2 - 2(1 - \nu)(w_{xx}w_{yy} - w_{xy}^2)]dxdy}{\int\int [N_n w_x^2 + N_y w_y^2 + 2N_{xy} w_x w_y]\, dxdy} \qquad (11)$$

where D is the flexural rigidity of the ribbon, ν is Poisson's ratio, N_x, N_y, and N_{xy} are the longitudinal, transverse, and shear stresses, respectively, which have been multiplied by the thickness of the ribbon, and $Z = w(x,y)$ is the buckled shape of the ribbon or, equivalently, the surface which satisfies the appropriate boundary conditions and minimizes the expression 11. The subscripts on w refer to its partial derivatives with respect to the indicated variables.

We examined the values of the denominator for some of the buckling models of the J181 growth configuration and found that the term involving the shear stress, $2N_{xy}w_x w_y$, was the major contribution to the integral and that this term was greatest near the melt surface. Although the term involving the x and y stresses directly are small (but not negligible), these stresses influence the buckled shape w(xy), and thus affect the term involving the shear stress.

As an example, compare the stress data in Figure 6 (Case 1A) with the data in Figure 13 (Case 2-2.50). Case 1A presents the results for a .015 cm thick ribbon, while Case 2-2.50 represents a .010 cm thick ribbon; otherwise the two cases are identical. If the stress patterns were identical, then equation 11 would require the buckling eigenvalues to be proportional to the square of the ribbon thickness: D has a factor of the cube of the ribbon thickness, while the N's have a single factor of the thickness. Thus, the eigenvalue of the .015 cm ribbon (Case 1A: $\lambda = 1.65$) should be 2.25 times as large as the eigenvalue for the .010 cm

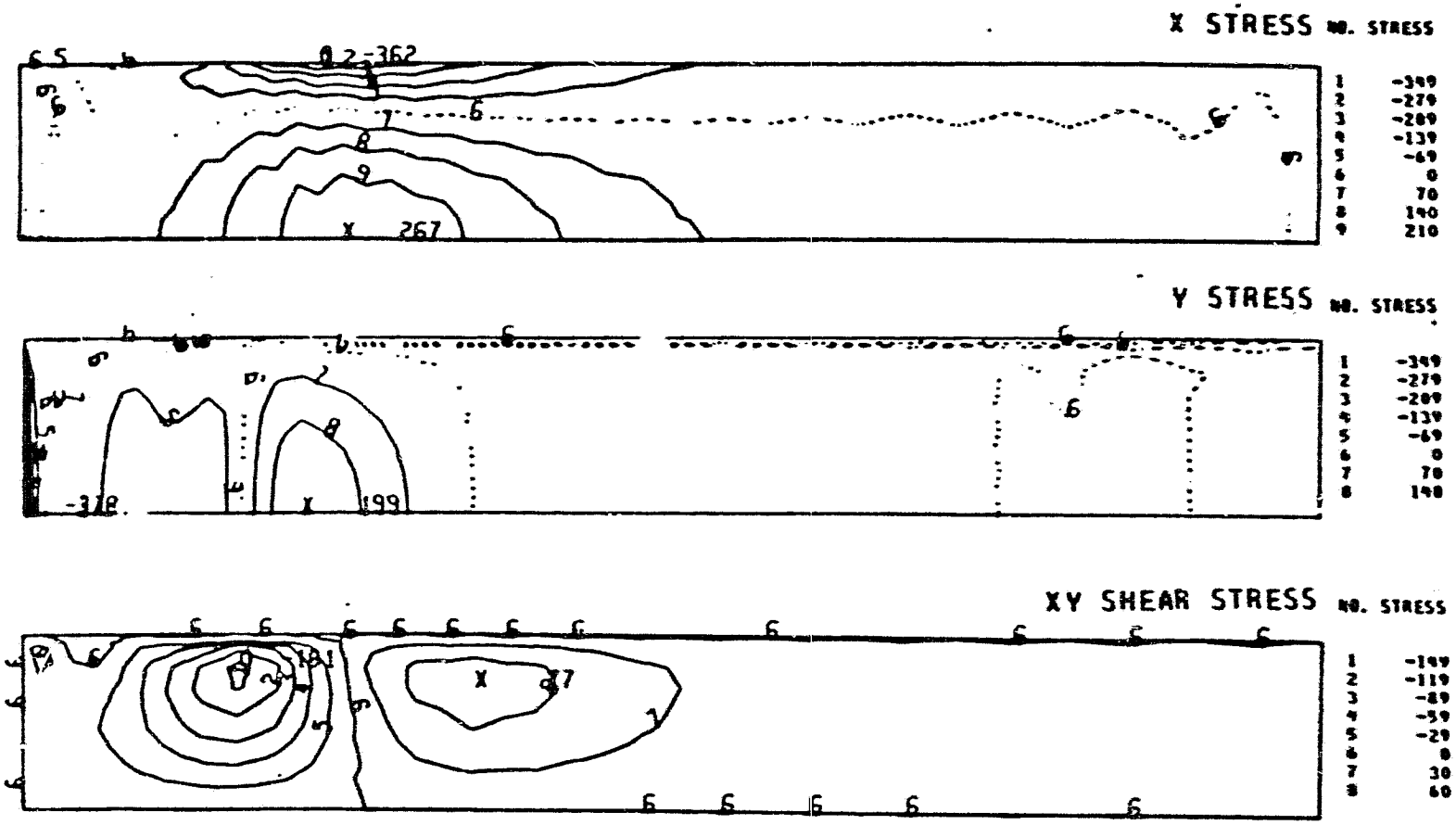

Figure 13 — Stress Patterns in .010 cm Thick Ribbon

ribbon (Case 2-2.50: $\lambda = 1.11$). The finite element buckling calculations show that this ratio is only 1.49.

One reason that the theoretical ratio of 2.25 is probably too large is that the dendrite size has been kept the same in both cases (.06 cm thick) and tends to dominate the stiffness factor, D. Even taking an average thickness gives a ratio of 1.79, still too large. Furthermore, the stress patterns are not identical for both cases. The temperature profile is slightly different for the two ribbon thicknesses and causes a slight change in the stress distributions. The differences in the maximum to minimum x-stress, y-stress, and xy-stress has changed by 8%, -4%, and -1%, respectively, for the .015 cm case, compared with the .010 cm case. The apparently most significant factor in the denominator of equation 12, the large negative shear stress, increased in magnitude by only 2%. This alone does not account for the ratio of the two eigenvalues; the changes in the stress patterns have changed the buckled shape significantly. Since the x-stress pattern had shown the largest increase in peaks and valleys, it is the most likely contributor to the larger-than-expected potential for buckling (smaller eigenvalue). The maximum and minimum x-stresses occur at the ribbon center line and at the dendrite and at about the same distance from the melt. Thus, the difference between the maximum and minimum x-stress is almost the same as the maximum of the Δx-stress defined as the difference between the x-stress at the centerline of the ribbon and at the dendrite at the same distance from the melt.

For the J352/J98M3C lid/shield configuration which will now be considered, the Δx-stress, x-stress, xy-stress, and the y-stress (away from the interface) patterns show approximately the same behavior with respect to the parameter variations under consideration. In other words, even though the Δx-stress pattern is not the only contribution to buckling, it is a good indicator for it since all the other stress patterns increase or decrease along with it for the cases we examined. While the y-stress near the melt is important for residual stress, it appears to be much less so for buckling.

3.1.4.3 Application to the J352/J98M3C Growth Configurations

The J352 and J98M3C growth configurations are two lid/shield configurations which have been used a number of times to grow silicon web crystals. Both configurations have some useful properties for web growth: the J352 produces crystals having very low residual stress, while the J98M3C, a width-limiting lid, produces constant width crystals having moderately small residual stress.

The web temperature profile is calculated as a one-dimensional problem, so that only the vertical geometry of the lid and shields is important. Furthermore, the resolution of our present thermal model, shown in Figure 14, is such that both the J352 and J98M3C configurations can be modeled by more or less the same geometry. In the model, the lid itself is more or less accurately represented as to thickness, slot width, and possible bevel and may also have a different slot temperature, TC, and top temperature, TS, a condition which would exist with a thin top shield very close to the top of the lid. In the model, however, the stack of shields above the lid must be represented by a lumped region of constant temperature, TAS, which must be chosen to approximate the effective temperature of the shield assembly. In the calculations which are discussed here, the geometrical factors were based on the actual lid and shield dimensions, while the effective temperatures were estimated from measurements of various lids and shields.

Table 1 shows the values of the various model parameters for six cases related to the J352/J98M3C growth configurations. In addition to the physical parameters illustrated in Figure 14, there is a model parameter, V, which estimates the growth velocity of the web (the moving frame velocity in the heat conduction equation). This velocity depends not only on the heat lost from the web itself, but also the latent heat lost to the supercooled melt, and must therefore be estimated before the model can be run. One of the model output parameters, VV, is the portion of V due to the loss of latent heat through the web itself. In

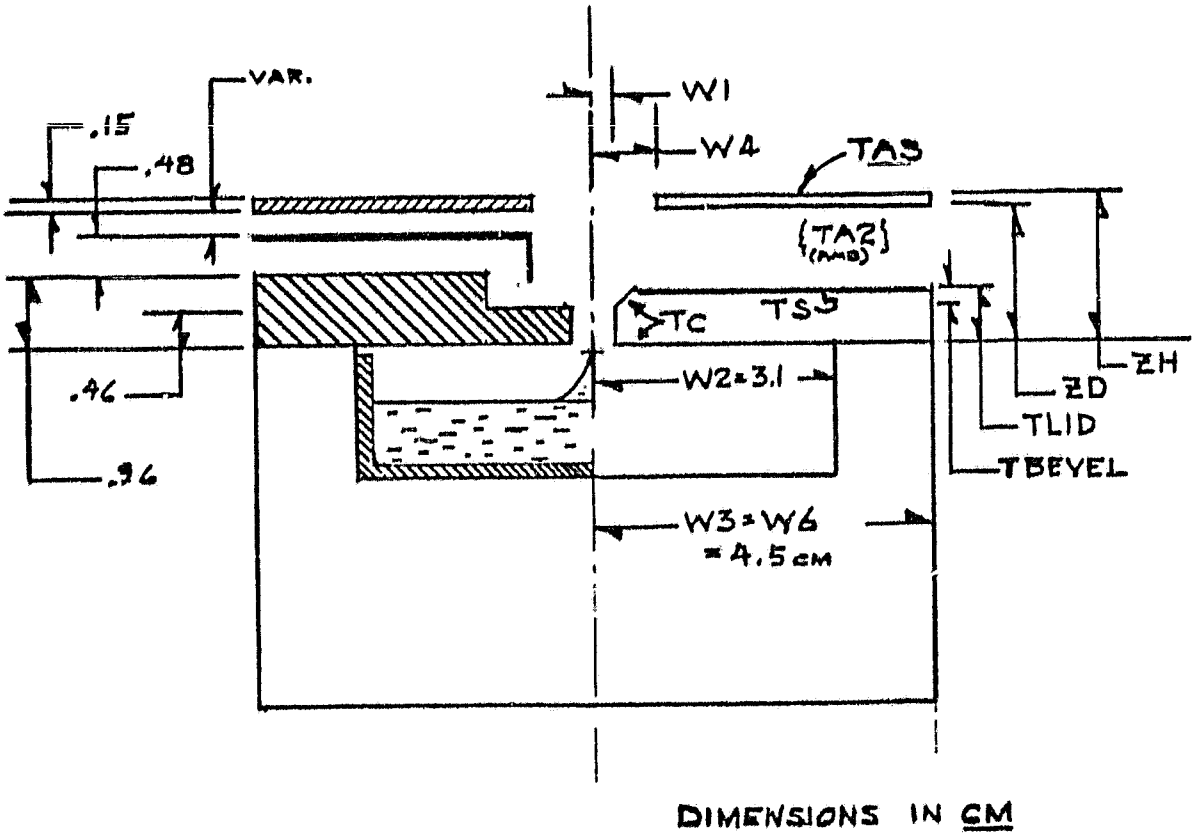

Figure 14 -- Schematic J352/J98M3C Configuration and Equivalent Thermal Model Parameters

addition to VV, the table also gives the Residual Stress Index, RSI, and the maximum Δx-stress.

Each of the cases listed in Table 1 has certain specific features which can be discussed individually.

Removal of top shield was simulated accidently in Case 10-1 by a numerical error in ascribing an input value of W_4 = 7.9 cm instead of 0.79 cm. This case modeled moving the top shield far from the lid, effectively removing it from the calculation. Case 10-3 is identical to Case 10-1 with the proper W_4 = .79. Comparison of the results shows several effects: 1) Stresses are larger and occur closer to the melt when the shield is removed, so that under that condition there would be an increased tendency to buckle; 2) the residual stress index is larger, so that there would be greater plastic flow near the interface; and 3) the web growth velocity is faster.

Melt level changes are modeled in Cases 10-2 and 1-3; in Case 10-2 the melt level is such that the growth front is at the same level as the bottom of the lid, while in Case 10-3 the melt level has dropped 0.1 cm. A comparison of the model output parameters shows that for the lower melt, the web component of the growth velocity decreased by about 20% and the maximum Δx-stress increased slightly, but that the Residual Stress Index changed by a factor of about 3.5. Thus, changes in melt height should have negligible effect on the buckling of the ribbon, a moderate effect on growth velocity (which has been observed) and a very pronounced effect on the residual stress.

Sensitivity to assumed growth velocity was tested by Cases 10-2 and 10-4. As discussed earlier, the moving frame velocity V is required as an input parameter for the integration, whereas the web velocity VV ($= K/\rho L\ dt/dx]_{x=0}$ where k = thermal conductivity, ρ = density, and L = latent heat of fusion) is calculated from the program. In Case 10-2, V was set at 2.0 cm/min while in Case 10-4, V was set at 1.5 cm/min; comparison of the output parameters shows that there are only negligible

Table 1 -- Model Parameters for J352/J98M3C

Parameter		CASES 10-1	10-2	10-3	10-4	10-5	10-6
(Input)							
TS	°K	1450	1450	1450	1450	1450	1575
TC	°K	1625	1625	1625	1625	1625	1625
TA	°K	300	300	300	300	300	300
TAS	°K	1175	1175	1175	1175	1175	1175
TA2	°K	1450	1450	1450	1450	1450	1450
B	cm	.015	.015	.015	.015	.015	.015
W1	cm	.3	.3	.3	.3	.3	.3
W2	cm	3.1	3.1	3.1	3.1	3.1	3.1
W3	cm	4.5	4.5	4.5	4.5	4.5	4.5
W4	cm	7.9	.79	.79	.79	.79	.79
W6	cm	4.5	4.5	4.5	4.5	4.5	4.5
ZD	cm	1.6	1.6	1.6	1.6	1.6	1.6
ZH	cm	1.75	1.75	1.75	1.75	1.75	1.75
TLID	cm	.8	.8	.8	.8	.8	.46
TBEVEL	cm	.25	.25	.25	.25	0	0
LIN	cm	.1	0	.1	0	0	0
V	cm/min	2.0	2.0	2.0	1.5	2.0	2.0
(Output)							
VV	cm/min	1.20	1.39	1.12	1.40	1.09	1.68
R S I		33.9	12.4	3.5	13.1	3.2	41.5
Max $\Delta\sigma_x$	Mdyn/cm^2	782	645	654	665	716	528

changes; hence, for velocities currently being calculated, the complication of iterative solutions is not warranted.

Lid bevel effects were brought out by comparison of case 10-5 with the standard case 10-2. Both geometries were identical except that the lid in Case 10-5 did not have the .25 cm x 45° bevel of Case 10-2. The effect of having the straight-sided slot was to slow down the web velocity, VV, and also to decrease markedly the Residual Stress Index. There was also some increase in the maximum Δx-stress, but this appears to be relatively small compared to the other changes.

Lid thickness was the final parameter investigated. Case 10-6 had the same geometry as Case 10-5, except that the lid was thinner: 0.46 cm instead of 0.8 cm. The result was that the thinner lid showed a marked increase in VV and also a large increase in the Residual Stress Index. The maximum x-stress decreased but, in addition to the main peak, developed a secondary peak nearer to the growth front. This second peak complicates interpretation of the results in terms of the tendency to buckle, and a complete buckling calculation would be necessary to evaluate the change.

Six conclusions can be stated from the modeling runs for the J352/J98M3C model reported in the previous section:

1. The presence of a top shield apparently reduces the thermal stresses in the ribbon -- both the RSI and the Δx-stress.

2. Lower melt level gives a lower RSI but does not affect the x-stresses further up the ribbon.

3. The calculations are insensitive to the pull velocity assumed as an input parameter, at least for a reasonable range of values.

4. The presence of a bevel on the susceptor lid can have a significant effect on the partial web velocity, VV, and on the thermal stresses.

5. A thin lid is likely to have a large RSI, albeit a larger web velocity.

6. The growth velocity and the thermal stresses are unrelated, although they may appear to be correlated if only one parameter is changed.

3.1.5 Zero Stress Profiles

We have seen that the J181 configuration produces a temperature profile along the ribbon that would cause sufficient stress to buckle silicon ribbon grown to a 31 mm width and 150 μm thickness. In order to redesign the lid and shield configuration to produce wider and/or thinner ribbon, we would like to know how the temperature profile could be modified to reduce stresses in the ribbon. A first step toward this goal is to find temperature profiles that produce no stress at all.

That a linear temperature profile should yield zero stress is derived from the equation

$$\Delta^2 \phi = -\alpha E \Delta T \qquad (2)$$

where ϕ is Airy's stress function, α is the thermal expansion coefficient, E is Young's modulus, and Δ is Lapalace's operator. For zero stress, the left-hand side vanishes and we find that $T''(x) = 0$, since T is a function only of the distance x from the melt and not of y or z (to a close approximation in ribbon growth). The above equation, however, was derived for constant α. For α a function of T ($\alpha = 2.8171 \times 10^{-6} + 9.789 \times 10^{-10} T$ for silicon), we replace the condition $T'' = 0$ by $(\alpha T)'' = 0$. One resulting temperature profile is shown in Figure 15, curve 9-1. This curve must pass through the point ($x = 0$, $T = 1685^{\circ}K$) and can be at any chosen temperature at the other end. However, if this temperature is reasonable, then the slope at $x = 0$ would be so small as to produce very slow ribbon growth. If the initial slope of this curve was chosen for reasonable speed, then the temperature at the other end of the ribbon would be so low as to be physically impossible. One way around this problem is to try to design for a "zero stress" temperature

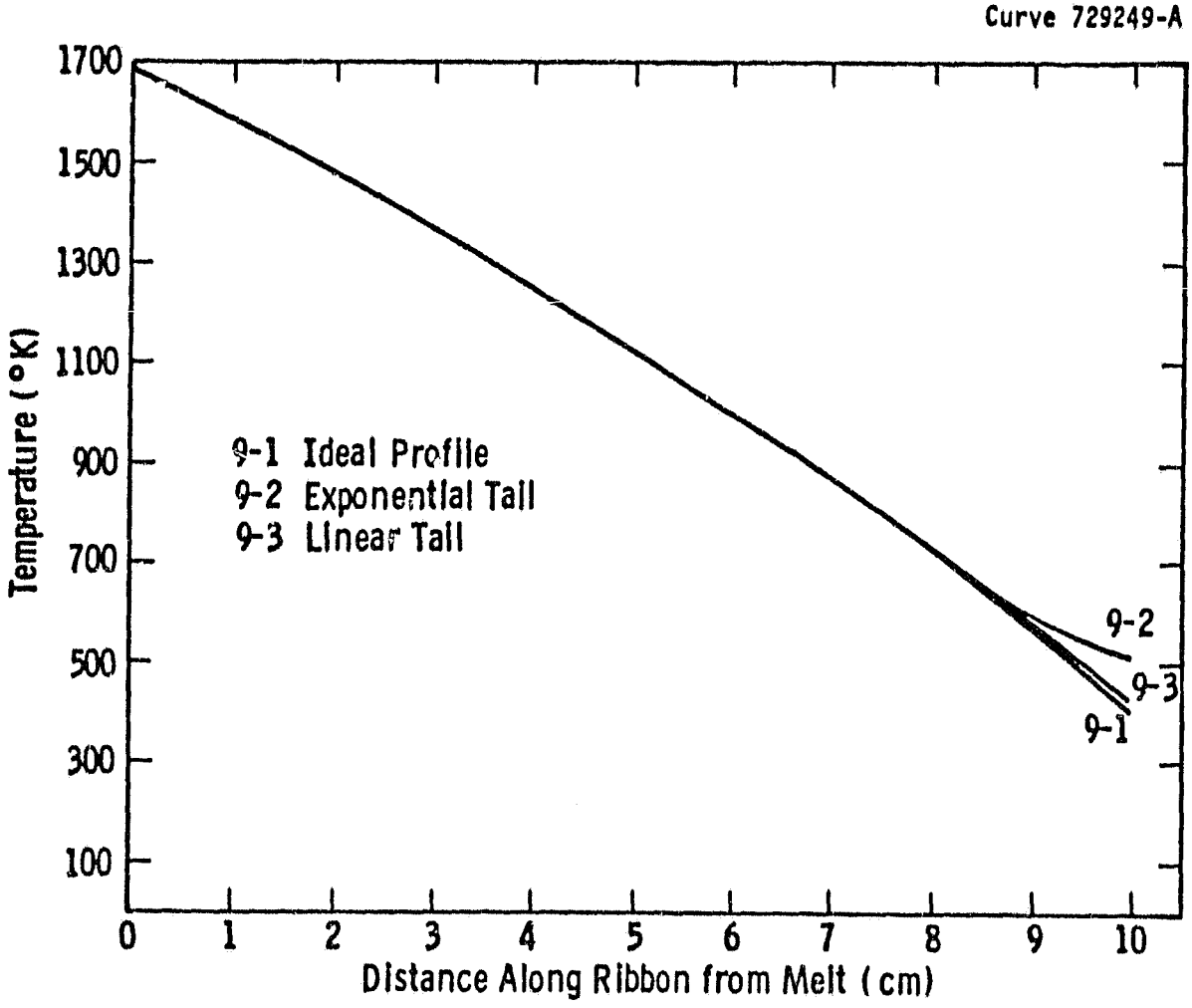

Figure 15 -- Synthetic Temperature Profiles

profile near the melt with a reasonable slope and then, at some point far from the melt, decrease the temperature at a much slower rate than that of the "zero stress" profile.

In Figure 15, curve 9-1 is a "zero stress" curve. At 8 cm from the melt, two "tails" were joined to this curve in such a way as to maintain a continuous first derivative. The "tail" 9-3 is linear and 9-2 is an exponential function of x.

Plots of the difference in longitudinal stress (σ_x) between the centerline and the dendrite edge for each of the three temperature profiles are shown in Figure 16. The linear tail, which is barely distinguishable from the "zero stress" tail, produces a small additional stress. The exponential tail produces a major stress peak at about 8.5 cm from the melt, although it is not nearly as strong as some of the J181 cases which peaked at close to 1000 Mdyn/cm^2. The "zero stress" profile appears to produce small stresses at both ends of the ribbon; this is an artifact of the model. For these three cases, an 8 x 100 mesh of linear, two-dimensional, finite elements was used to model the half-strip. The "zero stress" case was additionally modeled with a 5 x 23 mesh of cubic finite elements which have eight more nodes per element than the linear elements. The calculations using the cubic elements gave a zero stress over the whole ribbon length and incidently took much less computer time.

We have found that small deviations from the ideal "zero stress" temperature profile can produce major stresses in a ribbon. To understand and quantify this effect better, we plan to examine additional synthetic temperature profiles for stress generation. In particular, profiles with steeper slopes at the melt surface are required for reasonable growth speeds.

3.1.6 Temperature Data for Modeling Calculations

Thermal modeling of a web growth system requires lid and shield temperatures as input parameters to calculate the heat transfer between

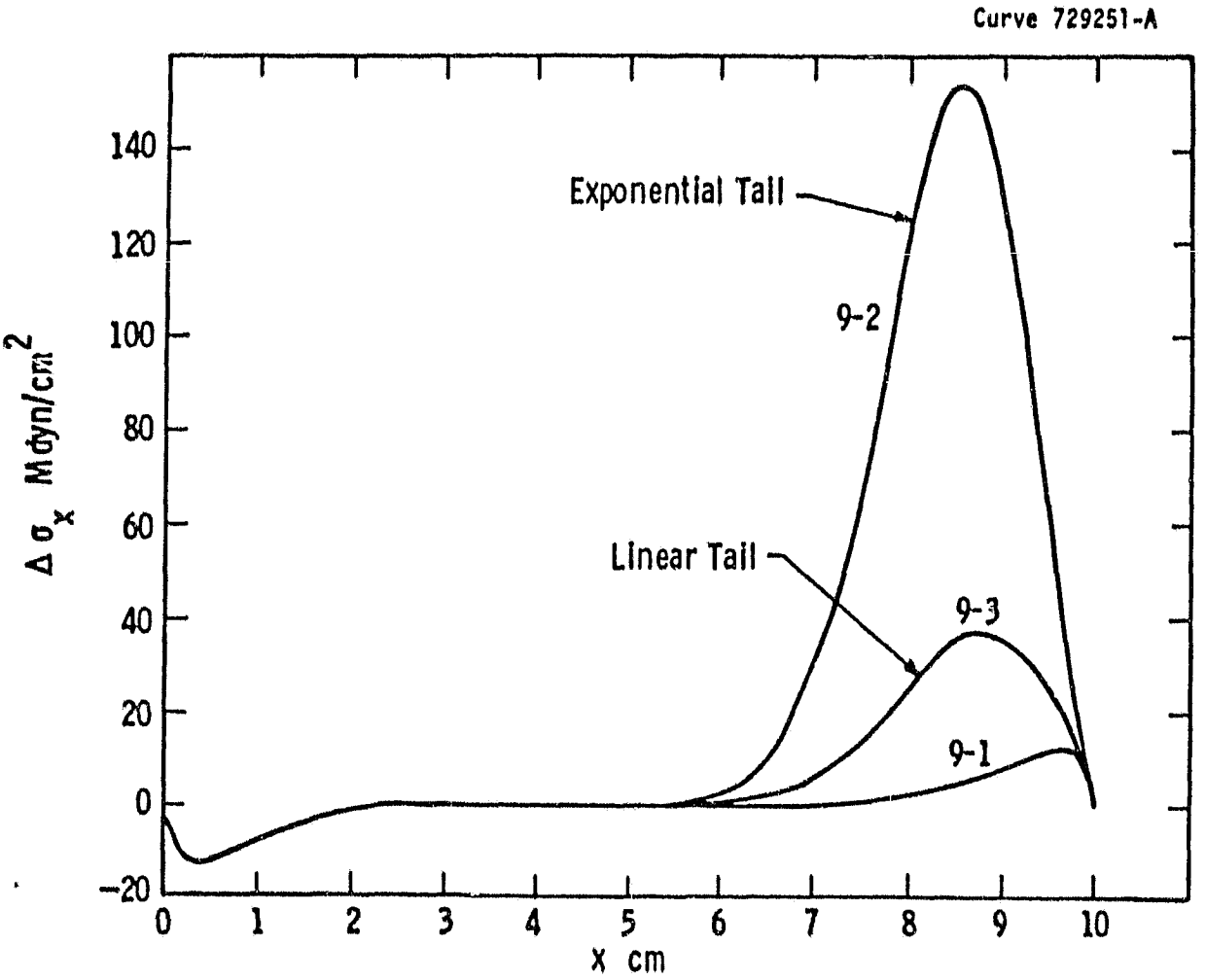

Figure 16 -- Comparison of Stress for "Ideal" and "Near Ideal" Temperature Profiles

the web and its surroundings. In most modeling work done so far, the necessary temperature data has been estimated from a limited set of measurements made on a J181 configuration some time ago.[9] Current modeling has become increasingly sophisticated so that more accurate and complete temperature data are needed. Not only are more extensive data needed, but also information is required as to the variation in temperature which can be obtained by adjusting the coil height and changing the coupling of the shields to the work coil, etc.

Two current growth configurations, the J352 and the J98M3A, were chosen for measurement since they are representative of many other configurations. The general lid and shield geometries are shown in Figure 17, which illustrates the configurations and shows the thermocouple locations. Additionally, two types of shields were used as the top shields in the J352 configuration: a normal shield which had a continuous edge and a slitted shield that had 1 x 12 mm slits every 12 mm along the periphery to reduce coupling with the work coil. Previous measurements had shown that such a slitted top shield ran significantly cooler than a similar solid shield, and additional information was needed.

3.1.6.1 Experimental Procedure

Shield temperatures, which were generally less than 1300°C, were measured with Type-K (chromel-alumel) thermocouples, while the lid temperature was measured with a Type-B (Pt/30%Rh -- Pt/6%Rh) couple. Small holes were drilled in both the lid and the shields and the thermocouple beads cemented in place with alumina cement to ensure good thermal contact. The thermocouple leads were brought through the furnace chamber wall with Conax compression seals. The Type-K leads were continuous to the measurement apparatus, while high-purity copper was used for extension leads with the nobel metal couple. The thermal emf's were measured and converted to temperature data by a Fluke 2240B Data Logger which also printed out the results at regular intervals.

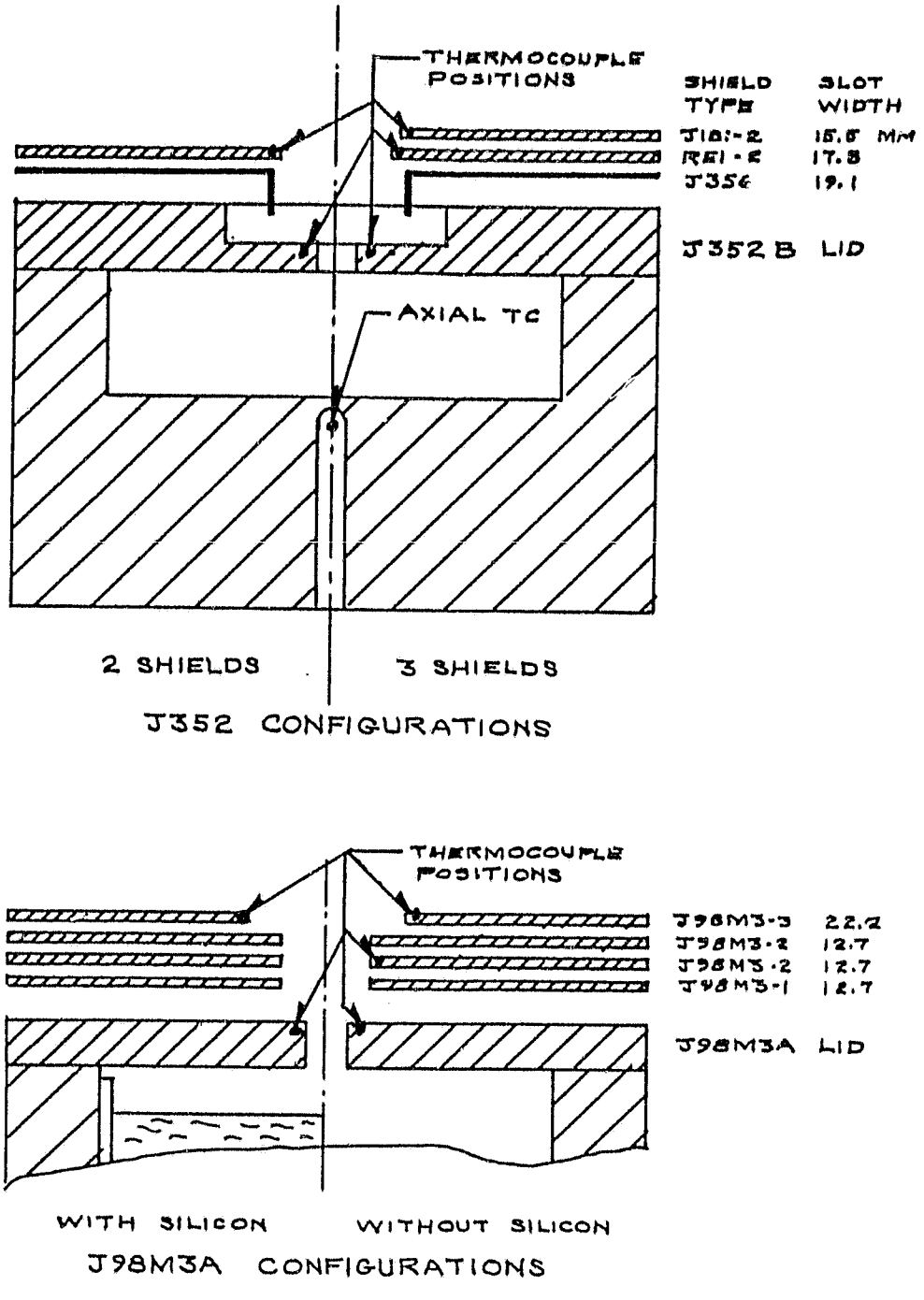

Figure 17 -- Configurations for System Temperature Measurement

Most of the temperature data were taken without silicon in the system so that a wide range of susceptor temperatures could be covered. For each configuration, temperature data were taken at three different coil heights and a range of susceptor temperatures (measured by a Type-B thermocouple on the axis of the susceptor). For the case of the J983A configuration, additional data were taken with a normal silicon charge in the system so that the lid and shield temperatures could be measured at the "hold" temperature to standardize the temperatures.

3.1.6.2 Results and Analysis

Measurements made without silicon in the system showed that the lid and shield temperatures were related linearly to the susceptor temperature over a wide range. Generally, the shield temperatures did not change as rapidly as the susceptor temperature; the lid temperature had nearly the same rate of change as the susceptor. Table 2 summarizes the measurements made on the various configurations shown in Figure 1. The data are expressed in terms of an empirical equation: $T = A + B(T_S-1380)$ [°C], where T is the element temperature, T_S is the axial susceptor temperature, and A and B are the fitting coefficients. The form of the equation was chosen so that A represents an approximation to the element temperature near normal operating conditions.

The coil position obviously affects all the element temperatures but has the least influence on the lid temperature. Slitting the edge of the top shield also has a strong effect on the shield temperatures, which shows that coupling with the work coil is a very important factor in determining the system temperatures. We attempted to analyze the lid and shield temperature distribution in terms of radiative transfer with an effective emissivity as the adjustable parameter. An emissivity on the order of 1.5 was needed to give even an approximate fit, again indicating that the inductive coupling was indeed a very important factor, even with the slitted shields. The results thus confirmed our assumption that measured, rather than calculated, temperatures were essential for accurate modeling predictions with real systems.

Table 2

Summary of System Temperature Data (Without Silicon)

$T = A + B (T_S - 1380)$

Configuration	Coil Height mm*	Lid A °C	Lid B	Bottom Shield A °C	Bottom Shield B	Top Shield A °C	Top Shield B
J352, 2 shields (top solid)	93.0	1324.9	1.0106			1031.4	0.7031
	97.5	1313.3	.8968			990.1	.7432
	102.0	1296.1	.7988			973.0	.3456
J352, 2 shields (top slitted)	93.0	1320.1	.8790			942.4	.7568
	97.5	1306.4	.8687			936.5	.8727
	102.0	1293.6	.8918			908.0	.7448
J352, 3 shields (top slitted)	93.0	1328.2	.9723	1144.8	.6573	944.7	.7146
	97.5	1319.5	.8702	1112.9	.6456	918.7	.7209
	102.0	1306.6	.8506	1075.7	.4183	883.2	.5618
J98M3A, 4 shields (top solid)	97.5	1334.7	.8694	1177.3	.7348	1033.7	.6174
	97.5	1322.3	.9379	1144.3	.7551	990.1	.5910
	102.0	1306.5	.9576	1107.5	.6202	936.3	.6573

*Coil height measured from arbitrary zero; smaller numbers are higher coil positions with respect to susceptor.

T_S is the axial susceptor temperature.

Experiments without silicon in the system give the data required to determine how the element temperatures change when the susceptor temperature changes. The presence of silicon permits evaluation of the element temperatures for actual operating conditions. Table 3 lists the lid and shield temperature data for a normal silicon melt at "hold" temperature for both the J98M3A configuration evaluated in the present experiments as well as the previously reported data for the J181 configuration (a three-shield configuration).[9] The data clearly show that the lid temperature has a relatively small range while the shield temperatures can vary widely. For example, in the J98M3A data, a 9 mm variation in coil height changes the lid temperature by only 17.6°C, while the shield temperature changes by 92.3°C. Furthermore, thicker lids run somewhat hotter: the 9.5 mm lid of the J181 runs about 25°C hotter than the 6.4 mm lid of the J98M3A. Thus, lid thickness provides a temperature parameter as well as a geometrical parameter for future system design.

3.2 Experimental Web Growth

3.2.1 Advanced Growth Studies

The objective of this activity is to develop the experimental understanding of web growth behavior in order to grow web crystals wider and faster, with the aim of achieving area growth rates up to 35 cm^2/min. This effort is tied closely to the thermal stress modeling effort.

There are two major aspects to this work: (1) developing lid and shield configurations giving higher growth speed at greater width and (2) developing the capability for steady state growth for long times.

The first activity is concerned with the continued design and testing of growth configurations which will permit both high-speed and low-stress operation, particularly low elastic stress which presently limits width through deformation of wide crystals. The second activity not only involves the design and validation of automated growth equipment, but also includes the achievement of growth configurations which

Table 3

Summary of System Temperature Data (With Silicon)

Configuration	Coil Height mm*	Lid Temperature °C	Top Shield Temperature °C
J98M3A, 4 shields (top solid)	93.0	1342.4	994.9
	97.5	1332.7	946.0
	102.0	1325.1	902.6
J181, 3 shields (top solid)	100.0	1354.7	963.1
	102.7	1351.3	941.7
	105.0	1344.6	927.4
(top slitted)	101.0	Open TC	876.6

*Coil height measured form arbitrary zero; smaller numbers are higher coil positions with respect to the susceptor.

produce a constant, controllable ribbon width compatible with melt replenishment.

3.2.1.1 Growth Velocity

During the early part of this period, experimental efforts were directed toward gaining a better understanding of the configurational parameters which affect growth velocity.

In order to increase growth velocity, a series of experiments with thinner lids was undertaken. A thin lid has the effect of increasing radiative losses from the web near the growth interface so that the heat of fusion is more rapidly dissipated, thus permitting more rapid growth for a given crystal thickness. Previous work had shown that simply thinning the lid, while having a large effect on growth velocity, can have negative effects in terms of crystal quality and oxide deposition. These effects occur because a thin lid tends to run colder in the region of the growth slot. Thus, concurrent changes must also be made in the top shield configuration in order to provide a vertical temperature distribution which not only produces substantially higher growth velocities, but also maintains good growth behavior in terms of growth initiation, crystal quality and freedom from oxide interference. To accomplish this, a series of experiments was undertaken in which the lid was systematically thinned in steps while changes were made in the top shield configuration to maintain good quality growth.

Initial experiments involved an RE-1[13] lid reduced in thickness by 20%, with the RE-1 shield arrangement. As expected, growth velocity increased significantly as determined by thickness-velocity measurements.[13] In terms of the relationship

$$V = c + \frac{d}{\sqrt{t}}$$

which relates growth velocity (V) to web thickness (t), both coefficients c and d increase when compared to the original thicker lid designs.

However, growth initiation was difficult and stability and crystal quality poor. The addition of two more top shields to this configuration resulted in stable growth with some tradeoff in maximum growth velocity.

Some other variations in the number and spacing of top shielding using the same lid have been tested. Only small effects were found in terms of growth velocity, but these experiments have led to the development of several important guidelines relating to lid and shield configuration which, if not considered, may produce unwanted side effects, for example, sporadic floating ice and growth-inhibiting oxide accumulation in the slot region of the shields. The configurational parameters to be controlled are the lid temperature and the spacing between the various components of the lid-shield stacks. By maintaining the bottom of the lid at sufficiently high temperature and keeping appropriate top shield spacing, oxide and ice are prevented.

The lid temperature can be controlled to the required degree by adequate radiation shielding and by proper positioning of the work coil. In addition, the lid bottom and susceptor top must mate well to insure maximum contact and thus maximum heat transfer between the two. When conditions are properly controlled in terms of shielding, lid-susceptor fits, etc., the lid bottom is totally free of oxide deposits, and ice from spalling does not occur.

One of the important aspects of top-shield spacing is the separation between the lowest shield and the lid. If this spacing is too small, oxide is deposited on the shields and grows out over the slot region, inhibiting crystal growth. The minimum spacing needed to prevent such oxide deposition appears to be about 4.5 mm. This observation had previously been made relative to the J-181 lid and shield configuration, in which the lowest top shield is thin and relatively cold. Recent experiments indicate that this spacing requirement is much more general and that the temperature per se is not the only factor to consider; the convective gas flow patterns are

critical in relation to growth-inhibiting oxide deposition on the top shields.

Another observation relative to shield spacing relates to the spacing between the individual shields in multiple shield stacks. A spacing of 1.5 mm is generally satisfactory. Expanding this spacing to 3 mm can cause the deposition of a hard blue oxide on the web crystal (as opposed to the normal, fluffy, easily removed type). Again, in this case the convective gas flow patterns are believed to be significant.

Even with improved shield spacings and lids which had reasonably fast growth speeds, growth was not always easy and crystal quality sometimes poor. In some cases, the crystals would degenerate after some tens of centimeters of growth. Split width measurements showed that some of the crystals had considerable residual stress, even at the relatively narrow width of 20 mm or so. These factors indicated that the lid temperatures in the vicinity of the slot were too cool, even with multiple top shields.

Another approach to achieving the proper thermal geometry was then tried: a thick (9.6 mm) lid with a recessed center portion around the growth slot. Such a configuration would have a higher slot temperature since the higher thermal conductance of the thick lid would transport heat more readily and, further, the thicker lid would couple to a greater extent with the work coil.

Several recessed lids with thicknesses in the slot region ranging from 5.6 to 3.2 mm have been investigated. The speed of these configurations is very similar to the speed of the flat lids of equal thickness, with the distinct advantage that the growth behavior is better. With each lid configuration a number of shield configurations has been tried. Two general types of configuration are shown in Figure 18. In the first configuration flat shields are used, but in the second configuration, one of the shields is made of thinner material and bent over to reduce radiative heating from the sides of the recess. An advantageous configuration uses the bent shield together with a top

Dwg. 7743A40

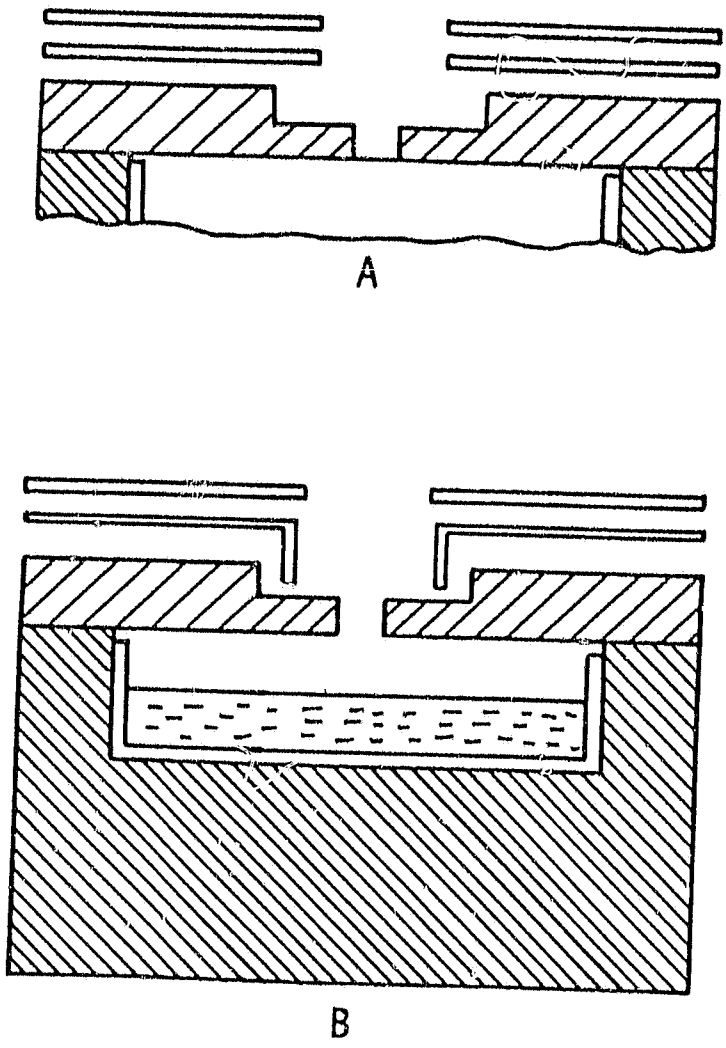

Figure 18 -- Typical Cross Sections of Recessed Lids for Growth Speed Enhancement

shield which is slitted around the edge to reduce coupling.[1] This combination provided relatively fast growth with an acceptably low residual stress, although other configurations were nearly as good. Although the shield configurations and the slot shape are very important in determining the speed of the system and its stress behavior, one of the most important parameters seems to be the melt height. Later in this report (Figure 31), data are given for the change in web thickness as a function of crystal weight (which is equivalent to melt height). Using the conversion that 20 gm of crystal is equivalent to 1 mm of melt height, it can be seen that significant speed improvement results when growth is maintained with high melts. Some of the configurations we tested have shown promise of such behavior.

The growth experiments with thin lids, recessed lids, and with a variety of shield geometries have reemphasized the large number of parameters which influence the growth behavior of dendritic web. All of these factors interact in a complex way to determine the growth speed and thermal stress in the growing ribbon. The experiments so far indicate that achieving any optimum configuration by empirical methods alone is difficult. It should be noted that the reduction in buckling stress through the utilization of the thermal modeling results will not only benefit crystal width, but also growth velocity through the thickness dependence; i.e., low stress permits high crystal quality to be maintained at lower thickness, and thickness and velocity bear an inverse relationship.

3.2.1.2 Width Control

For the continuous growth of long web crystals, it is necessary to limit or control the width at some desired value. In addition to targeting width to a specific size solar cell (reducing waste), the crystal width can be maintained below that at which stress-induced buckling might occur. Thus, very long crystals can be grown with the majority of the material usable for cell fabrication.

Configurations for width control were developed on an in-house program and utilized in this program where applicable. Data from an early crystal for which the width was controlled to within a fraction of a millimeter by passive lid design techniques is shown in Figure 19. Crystals have been grown to lengths over five meters at controlled width, without the benefit of melt replenishment.

3.2.1.3 Melt Replenishment

During web growth, a constant melt level is one of the requirements for maintaining constant thermal conditions, in turn required for steady state growth. Under the previous contract[1] a method was developed for detecting the silicon melt level and maintaining it during web growth; the feasibility of controlled melt replenishment over periods of many hours was demonstrated. On the basis of this experience, it was clear that a number of refinements was desirable in order to improve the melt level control function and to meet the requirements better for long-term semi-automatic growth, a goal of the overall design of the new experimental web growth machine. This improved system is described in Section 3.3. In this section, we will briefly discuss some of the experimental work related to melt replenishment.

During the period when the new melt control circuitry was being designed and constructed, growth experiments were carried out on the RE furnace using manually set replenishment rates.

Lid and shield designs which provide width control were adapted for replenishment by the addition of feed and laser holes. This enabled the melt level to be maintained reasonably constant using a constant feed rate. Any mismatch between feed rate and consumption rate is manifested as a thickness variation in the crystal, so that any needed adjustments in feed rate can be made empirically. Thus, growth at constant width allows growth experiments to be carried out at nearly constant melt level without the need for melt level sensing, at least over periods of several hours. It was also established that the

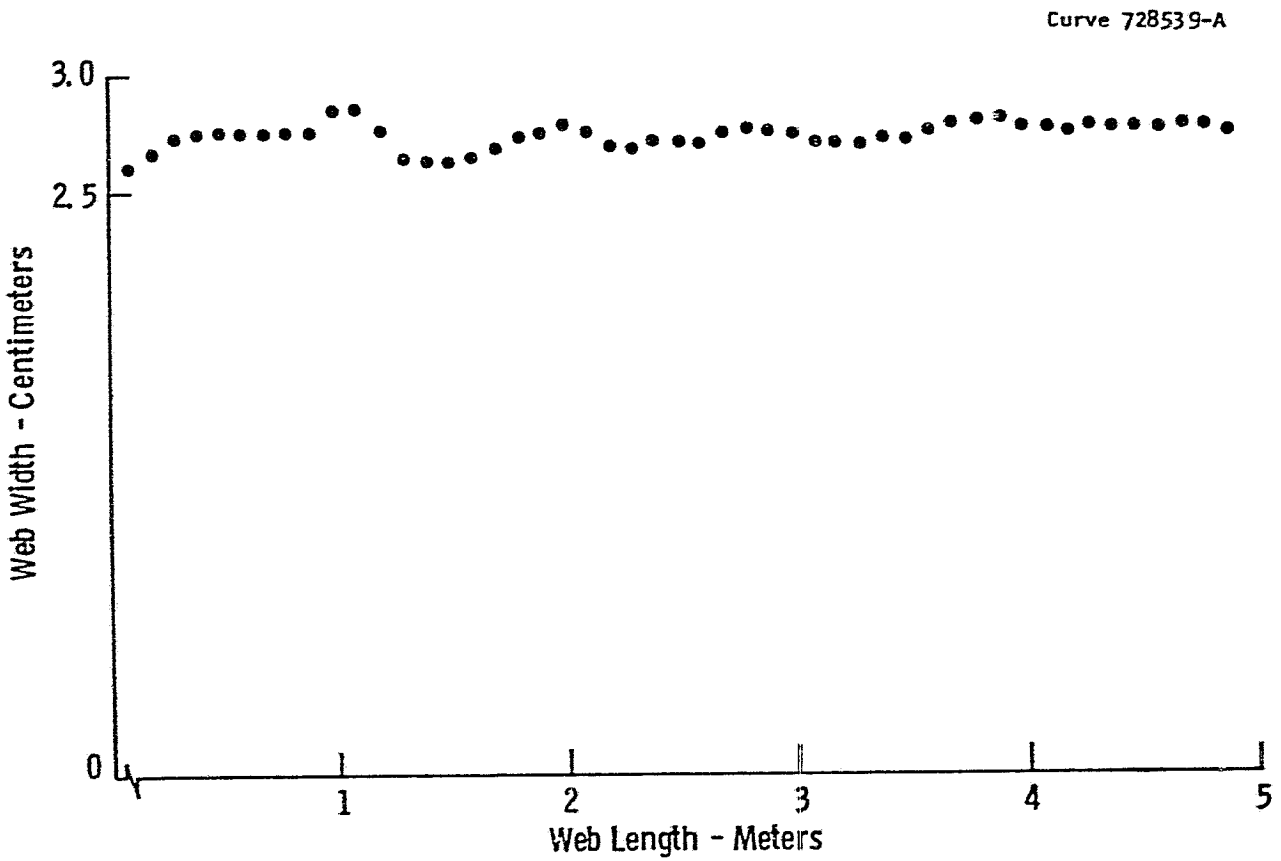

Figure 19 — Variation in Web Width with Length of Crystal Growth for Lid Geometry Designed for Width Control

width-limiting lid and shield designs continued to carry out their function in a melt replenishment configuration. Crystals up to four meters long were grown with manual replenishment.

Although the standard rectangular crucible design has performed well, it has become increasingly apparent that a longer crucible would be desirable in order to provide more physical space in which to separate the thermal requirements for growth of wide crystals and replenishment at the higher rates required to maintain a constant throughput. A new rounded-end crucible was designed and fabricated. This crucible has the same shape as the susceptor, i.e., the geometry follows the susceptor perimeter. This design adds nearly 5 cm of useful length along the crucible center line with no change in the furnace configuration except the shape of the recessed portion of the susceptor. Initial tests of growth behavior in the elongated crucible did not show any inherent problems, but the thermal characteristics of this configuration are somewhat different from those of the shorter rectangular configuration. The required shield positions, coil height, and crucible barrier positions for good growth with simultaneous replenishment were determined experimentally. The expected improvements in replenishment capabilities over the shorter crucible were indeed realized, i.e., increased thermal isolation of the feed and growth regions of the crucible. Pellets melted easily at more than twice the feed rate possible in the short crucible configuration without affecting crystal growth.

While this work was in progress, the new melt level control system was installed on the RE furnace and tested under growth conditions. Overall, the system operated as designed. This was established by recording both the output from the detector amplifier and the output from the motor controller (input to the pellet feed motor) and observing changes with changes in melt level. One modification deemed desirable was to lengthen the time constant in the control system in order to reduce the noise generated by the shimmering melt. In order to provide some flexibility in the choice of time constant, a circuit was designed

which provides a choice of 0, 20, 100, or 400 sec. This circuit was included in the melt level control system installed on the new experimental web growth machine.

Toward the end of this report period, the new experimental web growth machine was placed in service and operated on a regular basis. The facility functioned as intended, producing web in the first run. Part of the melt level sensing system had not yet been installed when these initial runs were made, so melt replenishment was accomplished with manually set feed rates. Replenishment at full replacement rates was carried out over the period of the work day without difficulty.

3.2.1.4 Programmed Start of Growth

A controlled and reproducible start-up sequence is desirable for reliable, routine web growth. It is also important to be able to isolate this variable in studies of crystal quality as a function of other growth parameters.

Typically, the growth initiation involves several minutes of coupled changes in melt temperature and growth velocity, as suggested schematically in Figure 20. The melt is first undercooled below the equilibration or "hold" temperature T_H to produce a button of suitable width. The growth velocity is increased to thin the button and start web propagation. Both temperature and velocity are then adjusted to their final steady state values. Small variations in the sequencing and rates of change in these manipulations can make the difference between "good" starts and "poor" starts. Thus, the quality and reproducibility of starts when performed manually is dependent on the skill of the operator.

Programmed start of the growth operation[3] has the potential for several important advantages compared to manual growth starts, including (1) repeatable wide starts, (2) reproducible high crystalline quality, and (3) less stringent operator skill and training. To

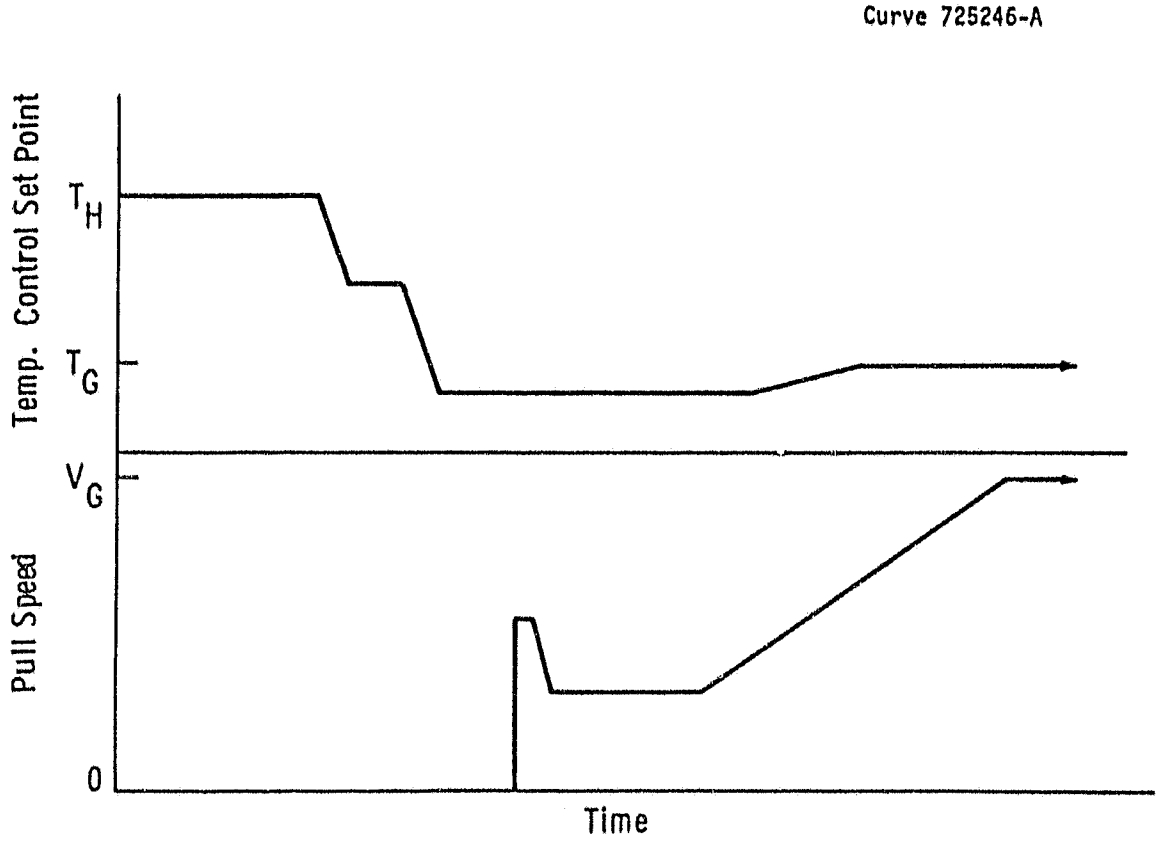

Figure 20 -- Typical Program Sequence for Web Growth Initiation

evaluate programmed start of growth, we have interfaced a Leeds and Northrup 1300 Process Programmer with the speed and temperature control circuits of a web growth furnace. This programmer features two synchronized programs which are independently set to adjust pull speed and temperature.

The system has been used to provide high-quality starts of growth with no operator input. The interfacing has been designed to allow synchronized ("bumpless") transfer from "manual" to "programmed" and back to "manual" status, thus permitting a single programmer to be transferred from furnace to furnace as required.

The circuits designed to accomplish the "bumpless transfer" between manual and programmed modes are depicted in Figures 21 and 22. In actual operation, the transfer from the remote or programmed mode to local, manual control is achieved by setting the voltage at V in each case to zero with the selector switch in remote. For temperature control, this is done by adjusting the alternate set-point potentiometer to match the output of the local set-point potentiometer. In the case of pull speed, the local control potentiometer is adjusted to match its output to that of the interface amplifier. The local/remote switches can then be set to local and the crystal growth maintained in the conventional manner throughout the rest of the run.

3.2.1.5 Long-Term Growth Stability

Unless compensated in some manner, a very gradual long-term temperature drift may occur during web growth. Without compensation, this temperature drift would eventually cause interruption of the web growth process, necessitating occasional restarting of the web crystal. Long-term drift occurs for at least two reasons: (1) gradual change of the temperature sensor calibration and (2) gradual change of the thermal properties of the system, notably the emissivity of heat shields.

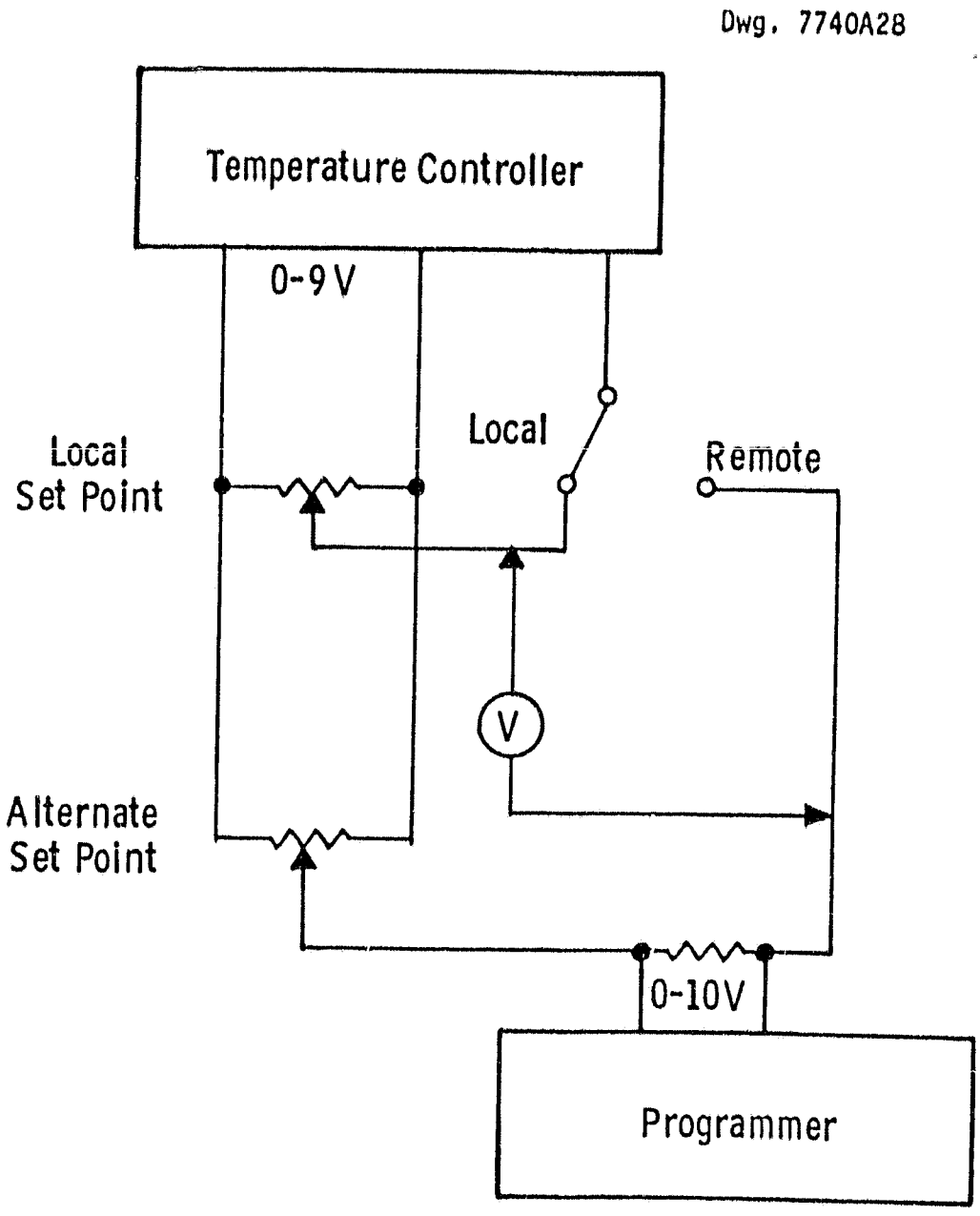

Figure 21 -- Temperature Control Transfer Circuit

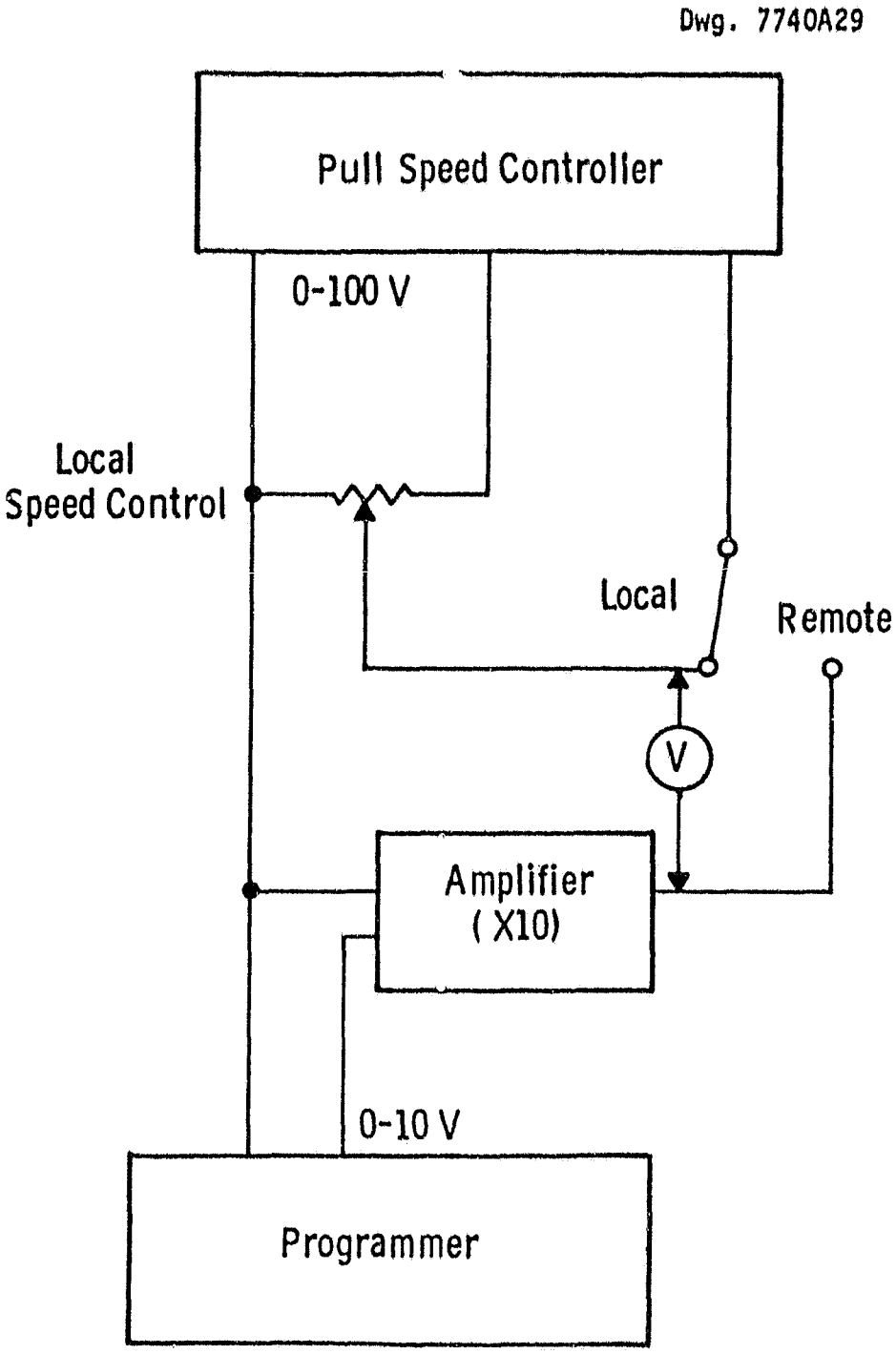

Figure 22 -- Pull Speed Transfer Circuit

We have tested two methods to sense and compensate the system for small thermal drifts, monitoring dendrite thickness and monitoring web width. Both methods work although we believe the latter approach offers some distinct advantages for control.

Dendrite thickness monitoring by visual observation has been in use for quite a while as a guide to adjust growth and is a sensitive indicator of the thermal conditions in the system. With the unaided eye or optical equipment, the dendrite is viewed edge-on; a thickening dendrite implies the liquid is too cold, a thin dendrite that it is too hot. Temperature adjustment can readily be made to compensate for drift due to sensor calibration change or heat shield emissivity variation with time. We recently attempted to quantify these observations by employing the use of a linear array of diode sensors coupled with an optical system to measure dendrite thickness.

EG&G RETICON manufactures such diode arrays and the associated circuitry and so was invited to Westinghouse R&D to demonstrate the equipment required. This equipment included the lenses needed to focus a magnified image of the dendrite on the diode array.

The demonstration was successful in generating a signal directly related to dendrite thickness. However, the light from the glowing melt was not adequate to obtain a well-defined image and an external light source had to be used. With external back lighting of the web sample in the furnace, an image of the dendrite having good contrast was obtained. With front lighting the image was discernible but the contrast was barely adequate. In both cases alignment of the optical system was quite important. Where back lighting was used, the orientation of the web was critical.

An alternative, and we feel better, method for temperature compensation is to monitor and control web width. Here the web is viewed face-on, a geometrically more favorable technique. With a suitably designed lid/shield configuration, our experience has shown that web width can be maintained constant within a fraction of a

millimeter so long as the temperature is constant. Thus, web width is a reliable indicator for temperature adjustments. Suitable optics can be used to enhance the width measurement.

Thus, we have concluded that width rather than dendrite thickness sensing is preferable for drift compensation. The method can be applied in the form of fully automatic closed-loop control or, alternatively, can be applied in the form of infrequent operator adjustment as needed.

3.2.1.6 Test of Feed Stock Pellets from Kayex Corporation

A sample of silicon in the form of shot made from semiconductor grade silicon was provided by Kayex Corporation. The pellets are roughly spherical with a diameter range of about 1.6 to 2.5 mm. In the first of two growth runs, the Kayex material was used for replenishment stock only, the original crucible charge being our standard polycrystalline silicon load. Growth behavior was normal during replenishment, and the pellets all melted readily in the crucible feed compartment. Because the holes in the pellet feed were far from optimum for the size of the pellets and the pellets were not screened to a narrow size range, multiple pellet drops frequently occurred. This was no problem, as the feed rate could be adjusted to a suitable average value, and no difficulty in melting was observed. However, by late in the day, all three feed holes in the pellet feeder became jammed with three pellets each and replenishment ceased. This problem could be readily solved with some adjustment in the pellet feeder hole size and some screening of the feedstock, particularly to remove "doubles" (two pellets stuck together).

In the second run, the crucible charge contained 31% of the Kayex pellets in order to test melting characteristics. The melt down was clean, with no trace of surface scum, indicating that the pellets were clean. (The pellets were used as supplied.)

On the basis of these preliminary tests, this material appears to be an excellent form for melt replenishment stock in the silicon web process.

3.3 Experimental Silicon Web Sheet Growth Machine

A new silicon web growth machine has been built and is ready for use in experimental web growth.

3.3.1 Purpose

The purpose of this machine is to support the experimental part of a program to obtain a fundamental understanding of the silicon web growth process. A fundamental understanding is required for evaluation of the technical feasibility and the ultimate commercial potential of the process. The program to achieve this understanding combines closely coordinated computer thermal modeling of the process and related experimental web growth. Until now, such an investigation was limited to experimental growth under transient conditions only. This new machine brings together, for the first time in a single machine, all of the growth control features developed by this program. With these features, evaluation of the fundamentals of the process can be performed under sustained steady state rather than transient conditions of growth.

3.3.2 General Description of Machine

The general configuration and placement of basic components of this machine, shown schematically in Figures 23 and 24, is not unlike that of web growth machines developed earlier in this program. These general features are described in the following paragraphs. New capabilities required for sustained steady state web growth, which are unique to this machine, will be discussed in a subsequent section (3.3.3).

As with earlier web growth apparatus developed under this program, web growth occurs within a water-cooled chamber (see Figures 23 and 24) which contains a protective (argon) atmosphere. In this chamber, the silicon melt is contained within a shallow quartz crucible which is, in turn, contained within an induction-heated molybdenum susceptor. Ten kilohertz induction heating is used principally because it permits

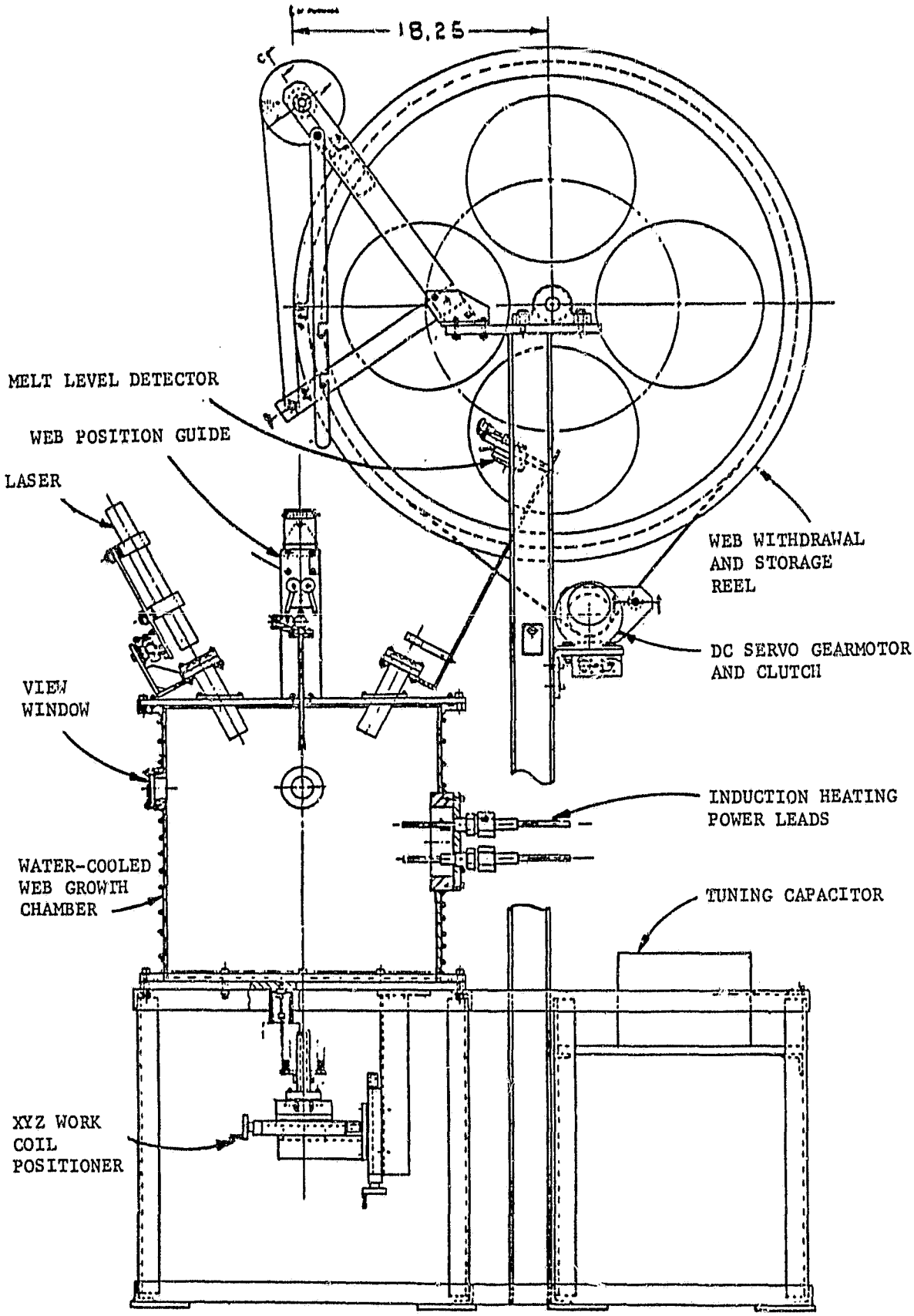

Figure 23 -- Experimental Web Growth Furnace -- Side View

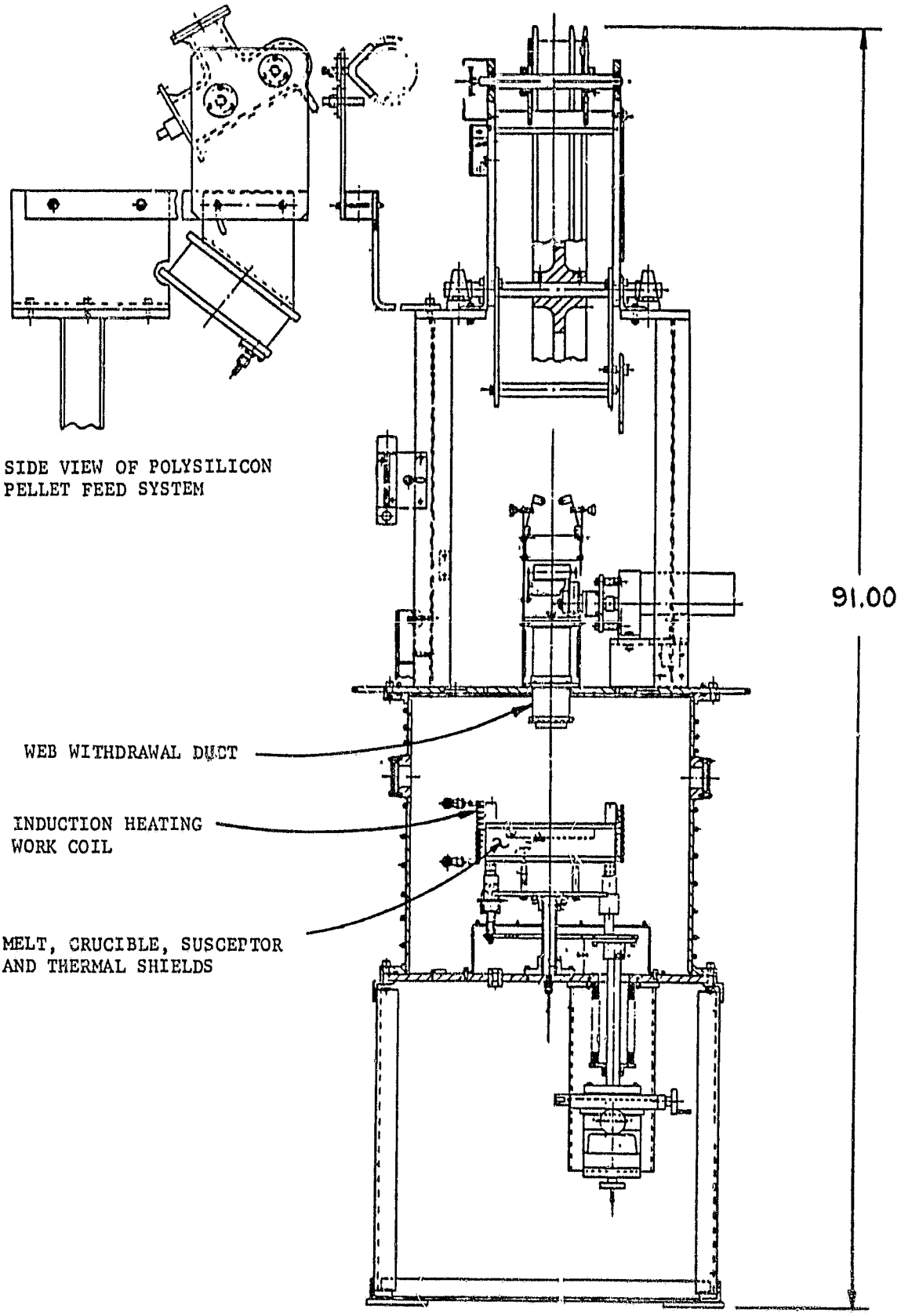

Figure 24 -- Experimental Web Growth Furnace -- Front View

freedom in the use of thermal shields with minimal induction coupling and an absence of voltage breakdown and corona. Temperature profiles within the melt and within the growing web are determined by a system of thermal shields which surround both the susceptor and the first several centimeters of growing web. An XYZ mechanical positioner for the induction heating work coil is situated below the growth chamber in the lower part of the furnace frame. The positioner is used to achieve front-to-back and side-to-side thermal asymmetry within the growth system, and to achieve the desired degree of dendrite penetration into the melt. These capabilities are necessary for experimental web growth with changing thermal configurations.

As the web grows it is withdrawn from the furnace through a duct into the room atmosphere. The geometry of the duct is essentially of a large length-to-area ratio such that only a small exhaust flow of argon is sufficient to prevent entry of room atmosphere into the growth chamber.

As the growing web exits the growth chamber and duct, it passes through positioning guides and winds onto the web withdrawal and storage reel. The linear speed of web growth is determined by the rotational speed of the reel, which is driven by a direct-current servo motor.

The speed and dimensional capacity of this machine is more than adequate to meet the area rate-of-growth goal for this program, as had been determined by economic analysis of the silicon web growth process. A photograph of the machine nearing completion of assembly is shown in Figure 25.

3.3.3 Required Features for Sustained Steady State Web Growth

The required features, applied simultaneously, permit web growth to attain a steady state condition of growth for periods from several hours to as many as several days. A growth period of several hours under steady state conditions is adequate for much of the fundamental study now in progress. A period of days, however, is required in order to appraise important long-term growth effects. This is important

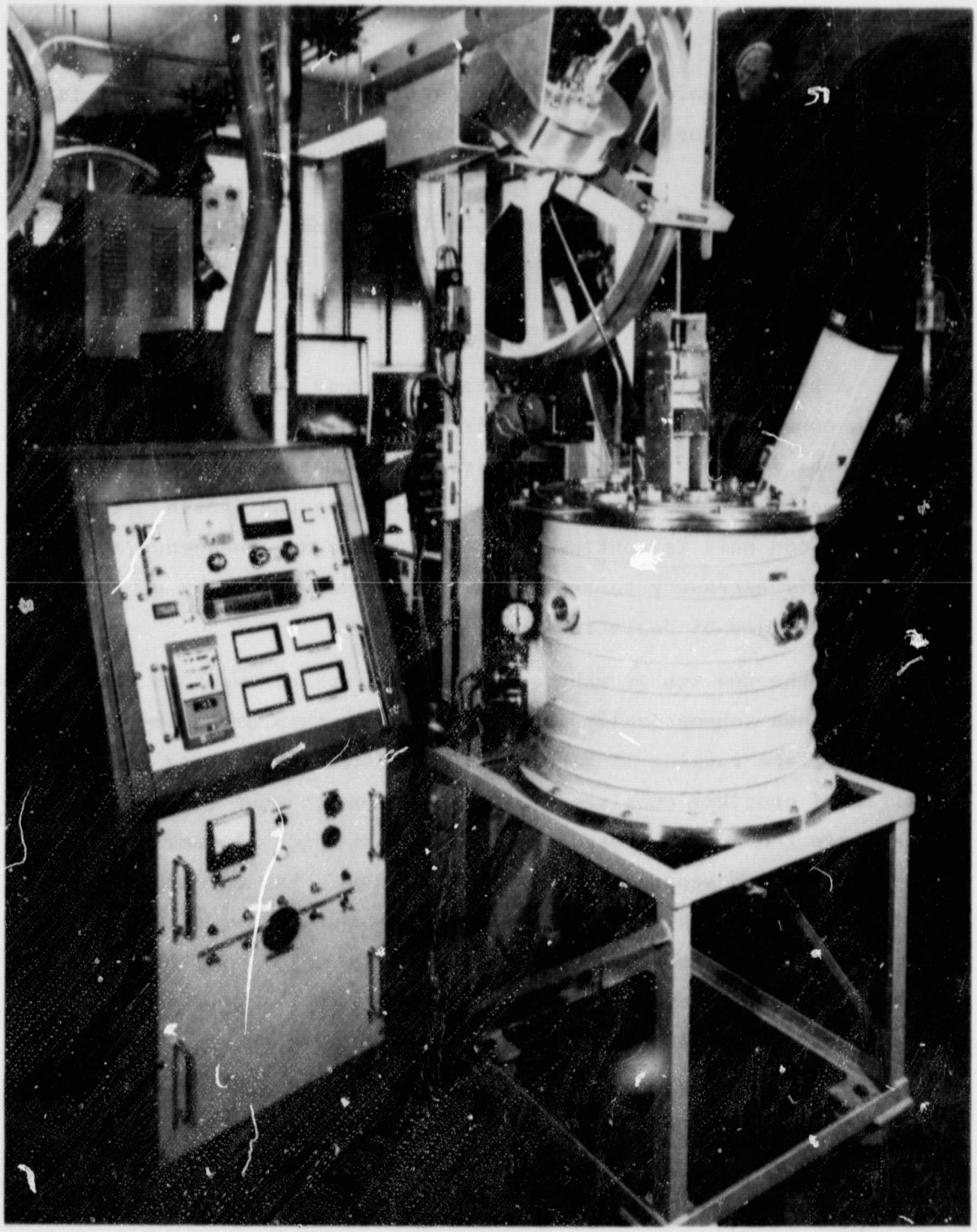

Figure 25 -- New Experimental Web Growth Furnace

because economic analysis has shown that a growth period of days is required in order for the process to become commercially competitive on a large scale.

The required features for sustained steady state growth are discussed in the following subsections.

3.3.3.1 Constant Melt Level

A basic requirement for sustained steady state web growth is to maintain constant temperature profiles within the melt and within the growing web. Because both profiles vary with melt height, it follows that the melt level must be held constant during web growth. Inasmuch as the silicon melt is continuously depleted as a consequence of web growth, it is necessary to replenish the melt continuously at a rate equal to the rate of depletion.

In the new web growth machine, melt replenishment is provided by a method shown schematically in Figure 26. In this arrangement, polysilicon pellets ranging in size up to three millimeters are fed into a partitioned crucible consisting of a small compartment into which pellets are fed and a larger compartment from which the web is grown. The barrier which separates the two compartments has an opening below the liquid surface which permits liquid flow and allows the liquid level to equilibrate in the two compartments continuously. The barrier does, however, prevent movement of unmelted pellets to the growth compartment where interference with web growth would otherwise occur. The barrier also prevents ripples from reaching the web growth interface as pellets are dropped into the melt replenishment compartment. Polysilicon pellets such as those (Figure 27) prepared by Kayex Corporation for a parallel JPL program have been found to work quite well with this melt replenishment system.

In order to maintain a constant melt level through use of the melt replenishment system, it is necessary to control the rate of pellet feeding such that it equals the rate of web withdrawal. To attain this

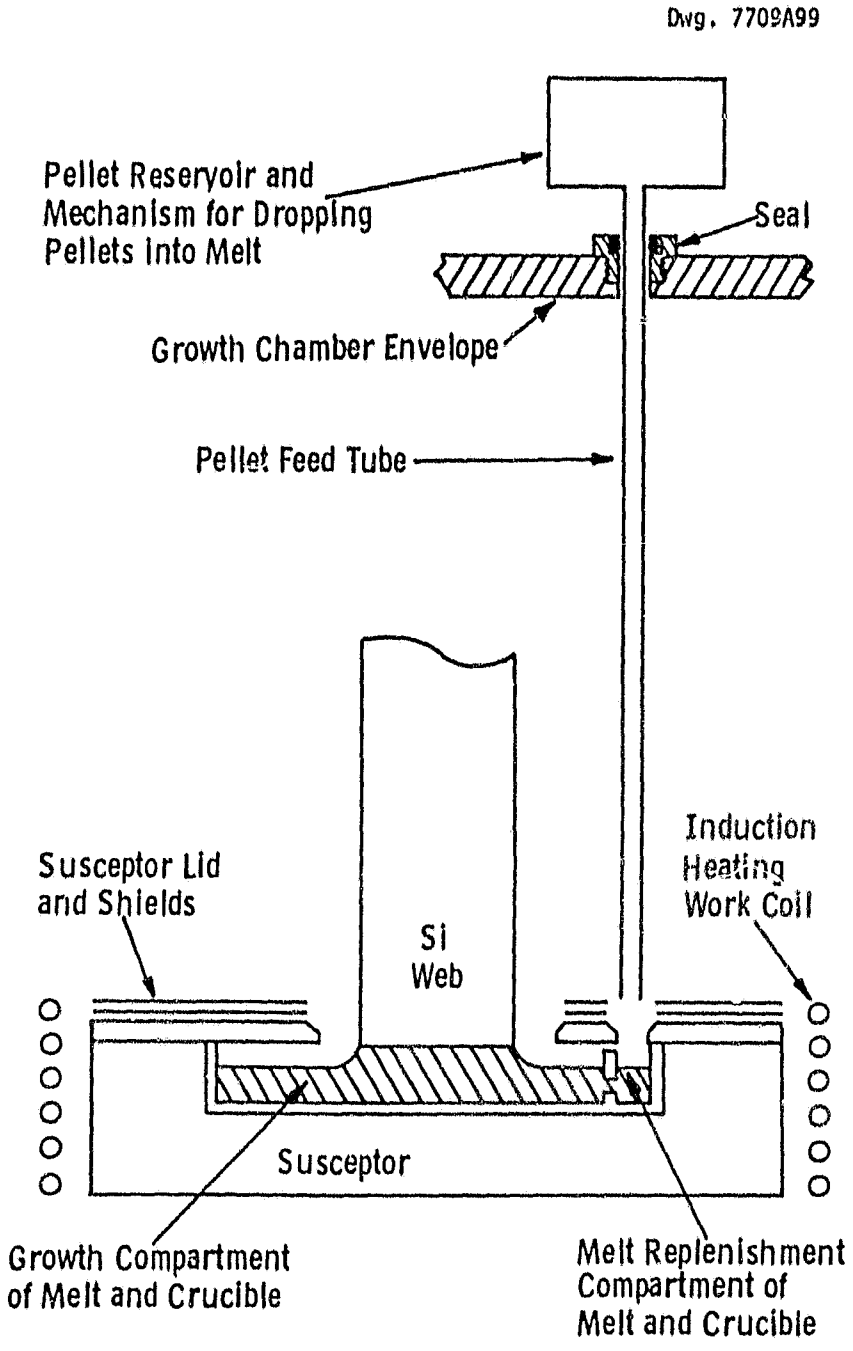

Figure 26 -- Simplified Sketch of Melt Replenishment System

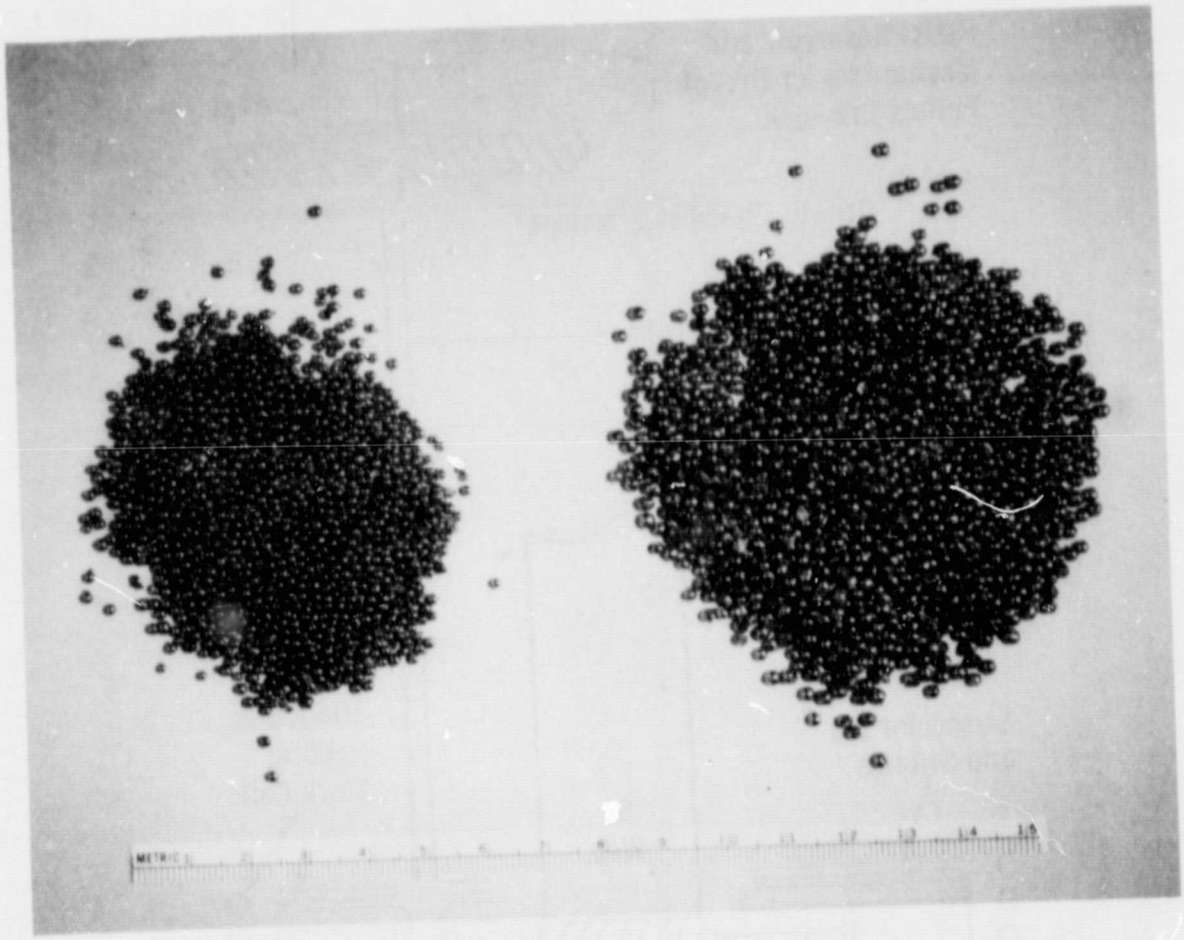

Figure 27 -- Polysilicon Pellets from Kayex Shot Tower. Left Side 0.4 to 2 mm. Right side 2.0 - 2.8 mm.

control a closed-loop melt level sensing and control system (Figure 28) has been developed for the experimental web growth machine.

For melt level sensing, this system utilizes a two milliwatt helium-neon laser mounted such that the light beam reflects from the melt onto a commercially available solid state position detector. The control loop is closed with circuitry (Figures 28 and 29) which measures the detector output and provides continuously variable speed control. This system controls the melt level to within 0.1 millimeter, the value which has been determined as the accuracy needed for steady state web growth.

3.3.3.2 Constant Temperature

Another requirement for maintaining constant temperature profiles (see Section 1.3.1) is to maintain a constant temperature at an appropriately selected location within the thermal system. The temperature sensor used for control is located within the wall of the induction-heated susceptor. Temperature control instrumentation in this application, similar to instrumentation used for low-frequency induction-heated Czochralski crystal growth, is shown in simplified schematic form in Figure 30. For this machine a fixed rather than adjustable range and zero offset are used. Temperature control accuracy obtained by this system is considerably better than the + 0.1°C range required by the web growth process for steady state growth.

3.3.3.3 Constant Width of Growth

For steady state web growth, the web output must be maintained constant in width, thickness, and speed of growth. Control of web growth width in the experimental web growth machine is attained by way of appropriate thermal design used in combination with the constant melt level feature described in Section 1.3.1 and the constant temperature feature described in Section 1.3.2. The thermal design maintains width within one millimeter and is developed for widths up to three centimeters.

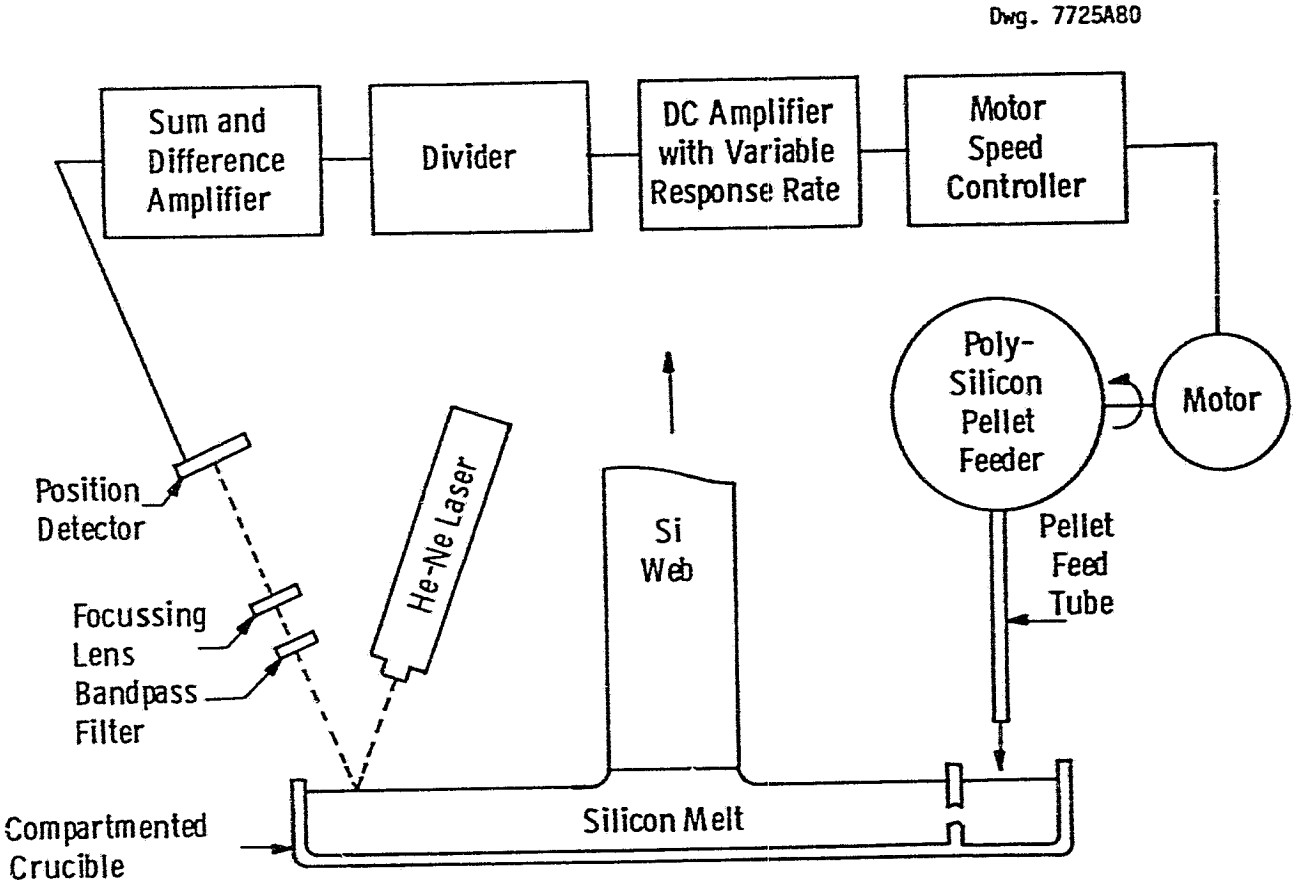

Figure 28 — Block Diagram of Closed-Loop Circuit for Control of Melt Level

Dwg. 7734A48

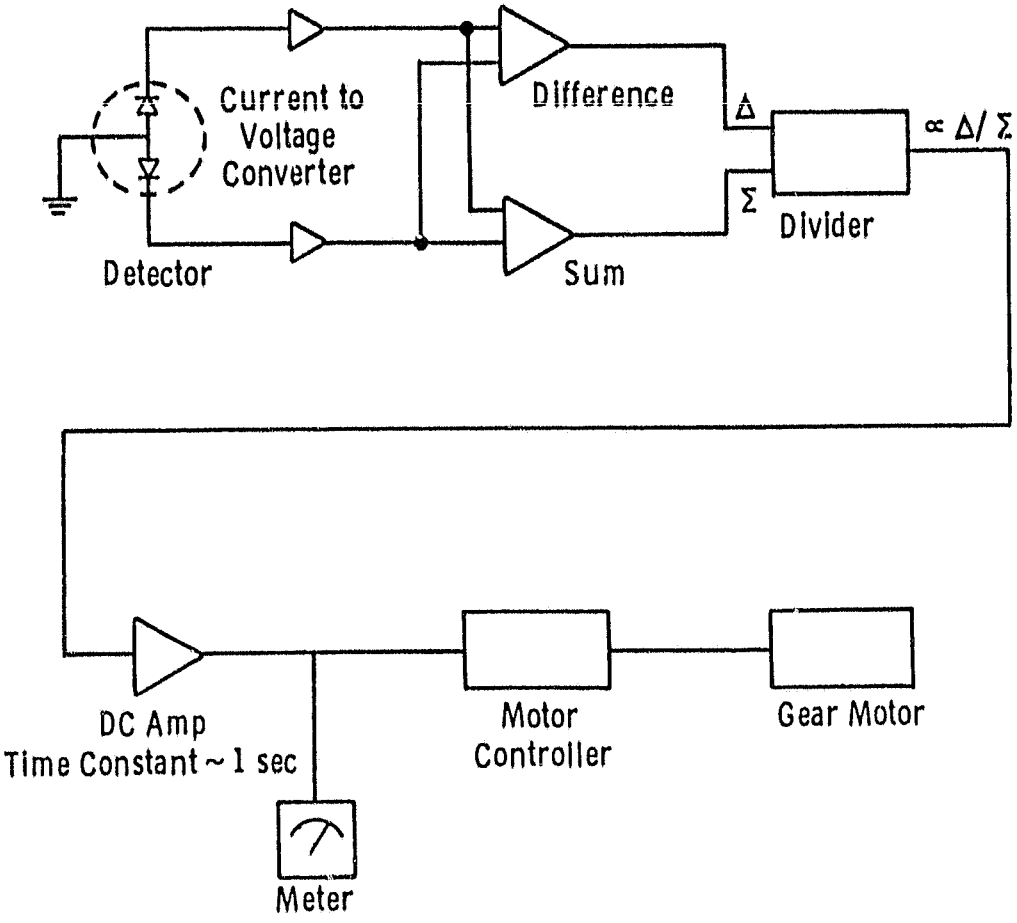

Figure 29 -- Block Diagram of Melt Replenishment Control System

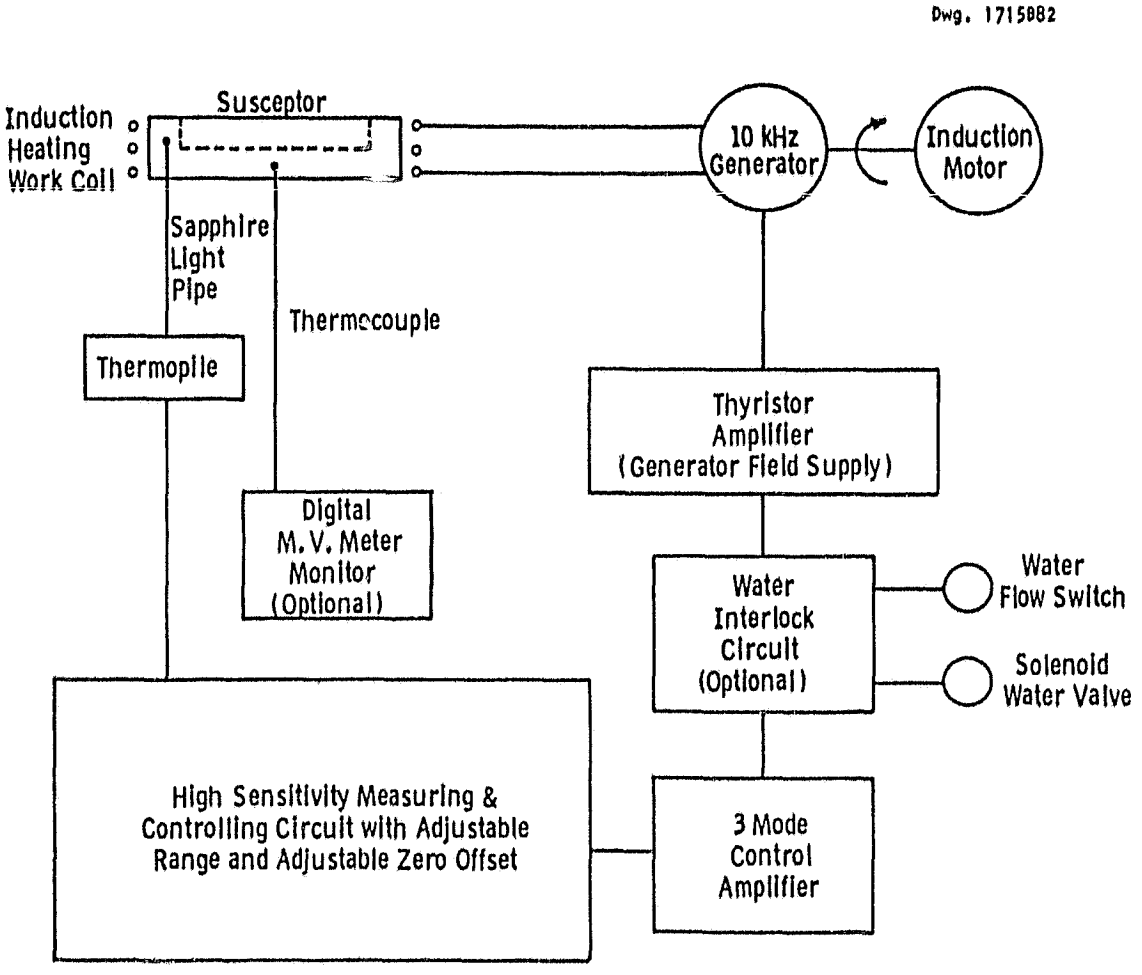

Figure 30 -- Block Diagram of Silicon Web Temperature Control System

The design will be modified to accommodate widths greater than three centimeters.

3.3.3.4 Constant Web Thickness and Speed of Growth

For any web growth thermal configuration, the growth thickness is a function of growth speed. This relationship will remain fixed for steady state conditions of web growth wherein the melt level and temperature are held constant. Thus, if growth speed is maintained at a constant value the web thickness will, consequently, also remain constant. The dependence of growth thickness upon melt replenishment (with constant temperature and melt level) is shown in Figure 31. For the experimental web growth machine, a dc servo motor is used to provide precisely constant reel drive and growth speed.

3.3.3.5 Programmed Start of Web Growth

Programmed start of growth is not a mandatory requirement for sustained solid state web growth. Manually started growth can and frequently does result in a high-quality web crystal. Manual starting nonetheless does have serious shortcomings in that it requires comparatively high skill by the web growth operator and, regardless of the operator's skill, frequently results in crystal imperfections which may ultimately lead to deterioration or failure of the web. Programmed start of growth has been found to eliminate essentially all of the manual start objections by producing good-quality, repeatable starts. The programmable start is a capability not yet fully utilized in that programs for highest quality and maximum width have not yet been developed. In the experimental web growth machine a two-channel commercial microprocessor-type programmer has been interfaced with the temperature and growth speed control systems.

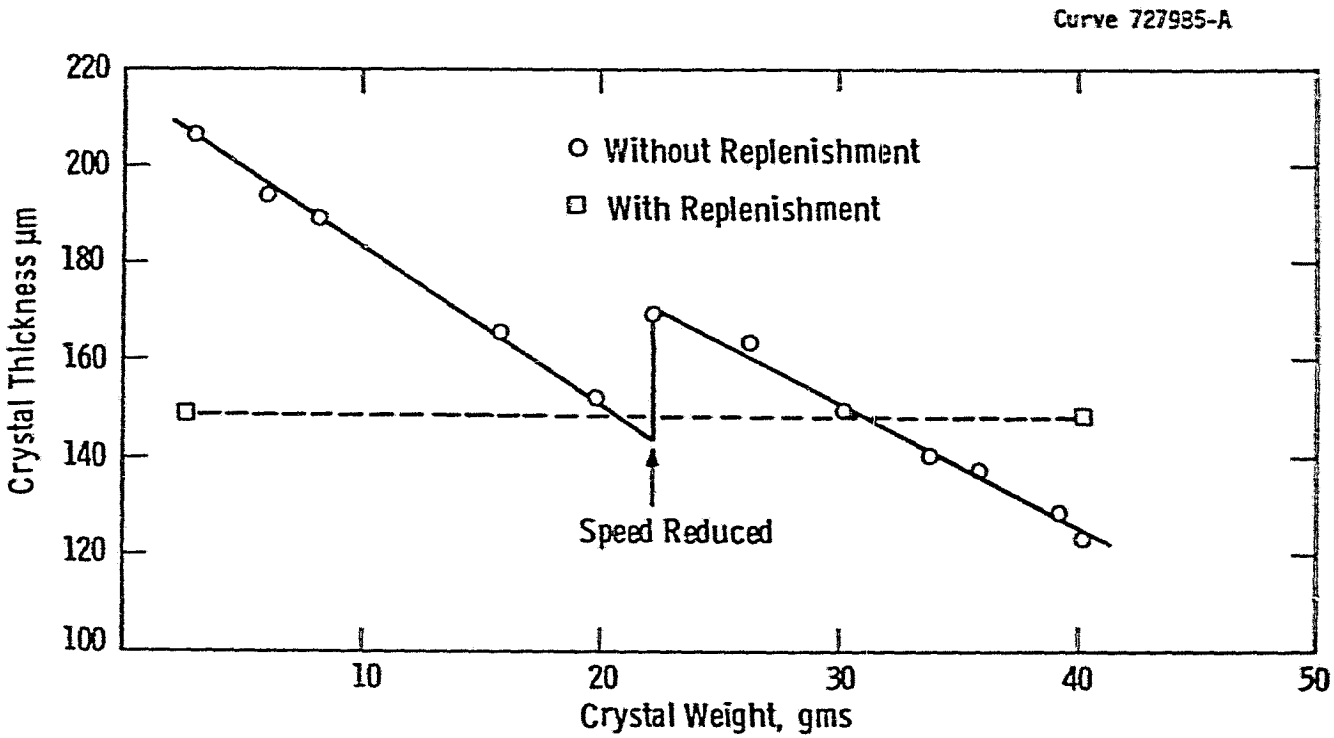

Figure 31 — Web Growth Thickness at Constant Growth Speed With and Without Melt Level Control

3.3.4 Summary

An experimental silicon web growth machine has been built and is now capable of satisfying all of the anticipated experimental needs of the on-going program to attain a fundamental understanding of the web growth process under conditions of sustained steady state growth. Such fundamental understanding is required in order that the process become commercially competitive. Experimental web growth with this machine will be closely coordinated with a parallel effort which models the web growth process and provides guidance to experimental work.

This machine is the first which combines all of the web growth improvements generated by this program. Each major component of the machine has been individually and independently proven prior to inclusion in the new machine. Coordinated experimental web growth will begin in the next reporting period.

4. SILICON WEB ECONOMIC ANALYSIS UPDATE

The basic input and assumptions of the IPEG economic analysis are unchanged. It has been deemed appropriate, however, to update the analysis in terms of comparatively minor cost corrections for crucibles, labor, and electric power. The adjusted costs shown are in 1980 dollars and include the following IPEG coefficients: EQPT-0.54, SQFT-110.6, DLAB-2.8, MATS-1.2, and UTIL-1.2. The cost breakdown for a three-day growth cycle is:

EQPT = .54 x $15,600	$8424
SQFT = 110.6 x 30	3318
DLAB = 2.8 x 4 hrs/run x $6.30/hr x 117 runs/yr	8256
MATS = 1.2 [$20+(68 hrs/run x $.06/hr)] x 117	3381
UTIL = 1.2 x 3kW x 68 x $.05/kWh x 117	1432
Annual cost per furnace	$24,811
QUAN (annual output per furnace)	1153M^2
Area cost = $24,811/1153	21.52/M^2
Value added cost = $21.52/(1000 x .15 x .95)	15.1¢/Wpk
Polysilicon cost at $14.00/kG	3.9¢/Wpk
TOTAL SHEET COST	19.0¢/Wpk

This projection of 19 cents per peak watt is 1.7¢/Wpk higher than the previous projection but well below the JPL 1986 goal of 22.4¢/Wpk.

5. SUMMARY AND CONCLUSIONS

5.1 Summary

The thermal stress model has been developed to the point where it can be applied to the design of experimental growth configurations. When applied to previously tested configurations, the model gave results in excellent agreement with experiment and is presently being utilized to design new low-stress lid and shield configurations which will be tested experimentally.

The value of the modeling effort cannot be over emphasized. Experiments have shown that in some cases, small differences in lid and shield configuration can have a large impact on both stress-induced deformation and residual stress in the web. Correlations between these effects and the results of calculations will enable us to concentrate experimental efforts on designs which the modeling results show to have a high probability for success.

The new experimental web growth machine has been completed. This facility contains all the functions necessary for long-duration, steady state web growth, including melt level control. Thus, growth experiments can be carried out with fixed thermal conditions. This facility has undergone preliminary testing and performed as designed, producing web on the first run. On the basis of these tests, some minor modifications in the melt level control circuitry were deemed desirable and these are being made. This facility, with the inclusion of low-stress, width-controlled lid designs, will enable us to carry out growth experiments under steady state thermal conditions controlled to a degree not previously possible.

5.2 Future Work

The thermal model for calculating temperature profiles in the web will be modified to incorporate more complex lid geometries and any number and shape of top shields. This will allow more complex configurations to be modeled accurately. Low-stress lid and shield designs will be developed, adopted for width control, and tested for long-duration steady state growth. This sequence will progress to wider web crystals grown at higher speeds as designs are improved.

6. NEW TECHNOLOGY

1. Programmed growth initiation of silicon web crystals, JPL New Technology items SC1293 and SC1295.

2. Thinner lids and improved shield configurations for greater throughput, JPL New Technology item SC1267.

7. REFERENCES

1. C. S. Duncan et al., Silicon Web Process Development -- Annual Report, June 30, 1980, DOE/JPL-954654-80/1, p 140.

2. R. G. Seidensticker and R. H. Hopkins, J. Crystal Growth, 50, 221 (1980).

3. R. W. Gurtler, J. Crystal Growth, 50, 69 (1980).

4. B. A. Boley and J.H. Weiner, Theory of Thermal Stresses (Wiley, New York, 1960), p. 261, 320-351.

5. S. P. Timoshenko and J. M. Gere, Theory of Elastic Stability (McGraw-Hill, N.Y., 1961), p. 348-351, 332, 367.

6. G. Fichera, "Existance Theorems in Elasticity," Handbuch der Physik VIa/2, (1972) 347389.

7. I. N. Vekua, New Methods for Solving Elliptic Equations (North-Holland, Amsterdam/John Wiley, New York, 1967) p. 247-254.

8. C. S. Duncan et al., Silicon Web Process Development -- Annual Report, May 31, 1978, DOE/JPL-954654-78/1.

9. Reference 1, p. 40

10. Reference 8, p. 195.

11. Reference 4, p. 345.

12. C. S. Graham et al., Final Report, Research Development of Low Cost Process for Integrated Solar Arrays, No. ERDA/SE/EC (11-1)-2721/FR/76/1.

13. C. S. Duncan et al., Silicon Web Process Development, Final Report, DOE/JPL 954654-80/13.

8. ACKNOWLEDGEMENTS

We would like to thank H. C. Foust, E. P. A. Metz, L. G. Stampahar, S. Edlis, W. B. Stickel, and W. Chalmers for their contributions to the web growth studies.